REDUCTION OF UNCERTAINTIES IN A 1D2D COUPLED HYDRODYNAMIC MODEL USING REMOTE SENSING DATA

ANTARA DASGUPTA

March, 2015

SUPERVISORS:

Dr. Praveen K. Thakur (First Supervisor – IIRS)
Mr. Prasun K. Gupta (Second Supervisor – IIRS)
Dr. Ing. T. H. M. Rientjes (First Supervisor – ITC)
Prof. (Dr.) V. G. Jetten (Second Supervisor – ITC)

REDUCTION OF UNCERTAINTIES IN A 1D2D COUPLED HYDRODYNAMIC MODEL USING REMOTE SENSING DATA

ANTARA DASGUPTA

Enschede, the Netherlands, March, 2015

Thesis submitted to the Faculty of Geo-Information Science and Earth Observation of the University of Twente in partial fulfilment of the requirements for the degree of Master of Science in Geo-information Science and Earth Observation.
Specialization: Natural Hazards and Disaster Risk Management (Hydrometeorology)

SUPERVISORS:
Dr. Praveen K. Thakur (First Supervisor – IIRS)
Mr. Prasun K. Gupta (Second Supervisor – IIRS)
Dr. Ing. T. H. M. Rientjes (First Supervisor – ITC)
Prof. Dr. V. G. Jetten (Second Supervisor – ITC)

THESIS ASSESSMENT BOARD:
Prof. Dr. Ir. M. G. Vosselman (Chair)
[Dr. N.N. Rai, (External Examiner, Director, Central Water Commission, GoI, New Delhi)}
Dr. Praveen K. Thakur (First Supervisor – IIRS)
Mr. Prasun K. Gupta (Second Supervisor – IIRS)
Dr. Ing. T. H. M. Rientjes (First Supervisor – ITC)
Prof. (Dr.) V. G. Jetten (Second Supervisor – ITC)

For Ma and Baba;

Shri Shankar Dasgupta

Smt. Amita Dasgupta

ABSTRACT

Dhanua River is a man-made flood diversion channel, which drains excess water from the Kushabhadra River in the Lower Mahanadi Basin, near the delta region of the river. The study has experienced three flooding events of high magnitude in the last 15 years (2003, 2011 and 2014) and is plagued by smaller floods almost annually. Additionally, the hydrological knowledge on the causes of such widespread flooding due to this channel was lacking, mainly due to the unavailability of any hydrometric gauges in the area. This data scarcity made setting up flood models for this channel scientifically challenging. This study aimed at analysing the flooding properties and reducing the uncertainties in the hydrodynamic model simulations. The paucity of hydrometric data was supplemented with satellite observations. The discharge hydrograph for the upstream boundary condition was calculated from gauge information available much further upstream, using water distribution information for the tributaries and the side weir formula in HEC-RAS. A hydraulic free flow condition was assumed at the downstream boundary condition and the flood model, MIKE FLOOD was calibrated using inundation extent observable in satellite data. Synthetic Aperture RADAR (SAR) data (RADARSAT-II and RISAT-I) was used to generate the flood maps, using three techniques, namely visual interpretation, histogram thresholding and texture based image classification using the variance and homogeneity filters. CARTOSAT – I stereo-pair of images was used to generate a high resolution 5m DEM which was used to interpolate the different resolutions used for the study. A detailed land use map was derived from high resolution multi spectral data from LISS IV for the distributed parameterization of the floodplain friction. The model MIKE FLOOD was used to simulate the flooding for the test site at a grid size of 15 m. The flood model was tested for parameter sensitivity and then calibrated for the roughness coefficients (channel and floodplain). The calibration was carried out on the basis of three spatial objective functions model bias, F (Over-prediction), F (1) (Correct Wet) and reliability diagrams. After validation the final values of model fit were found to be 0.415 (F), 0.143 (F (1)) and the model had a bias of 1.369. The R^2 value for the validation was found to be 0.938 and the RMSE was equal to 0.278. Two major flooding events were selected for this study, 04 September 2003 for model calibration and 09 August 2014 for validation. It was found that the model is extremely sensitive to both channel and floodplain friction but the flood plain friction had a greater impact on the spread of the inundation. The elevation uncertainty for DEM was constrained to $\pm$ 2.53 m for the simulated flood event, the parametric uncertainty of the bed friction to 0.0375 $\pm$ 0.00171 (Manning's n) and that of the flood plain friction to 44$\pm$2 (Manning's M). It was found that increasing the DEM resolution causes the simulation time to increase drastically (3 days for 5m and 14 hours for 15 m). However, coarser resolution DEMs were unable to constrain the flooding problem.

Keywords: Hydrodynamic flood modelling, MIKE FLOOD, SAR, DEM optimization, uncertainty.

ACKNOWLEDGEMENTS

First and foremost, I would like to thank my parents who have been supporting me consistently throughout my life in all my endeavours. I am grateful to god for giving me such a wonderful family and such a great opportunity.

I would like to express my sincere gratitude to Indian Institute of Remote Sensing (ISRO) and Faculty of Geo-Information Science and Earth Observation, ITC, Netherlands (University of Twente) for giving us this unique opportunity of experiencing the Dutch education system through this Joint Education Programme (JEP).

Special thanks to my supervisors at IIRS, Dr. Praveen K. Thakur for his critical comments and constant encouragement and Mr. Prasun K. Gupta for ensuring at every step that my work remains scientifically impeccable. Your guidance and advice were of significant help in the completion of this thesis.

I would like also like to thank my ITC supervisors, Dr. Ing. Tom Rientjes for making me keep it real and for helping me to set achievable targets for myself, as well as Prof. Dr. V. G. Jetten for constantly inspiring me and taking out time for my work even with his busy schedule.

I am especially grateful to our course coordinators, Dr. P. K. Champati Ray at IIRS and Dr. N. A. S. Hamm at ITC, for the constant help. You guys were there for us through everything, never belittled our insignificant problems when we brought them to you and stood up for us whenever we needed you. Your benevolence helped through our struggles and for that I am eternally thankful.

Special thanks to the Water Resource Department at IIRS. Dr. S. P. Aggarwal for providing us with all the necessary data and facilities, imperative for the completion of this research. Dr. Vaibhav Garg for helping me stay calm and carry on when my data purchase was delayed in the absence of my supervisors. Suruchi, Sahil sir, Ankur sir and Arun, you made the long working hours in the lab a lot more fun.

Special thanks to the Water Resources and Environmental Management Department at ITC, Dr. Suhyb Salama, Dr. Rogier Van der Welde, all the faculty and staff and all my colleagues, Marc, Ignace, Amie, David and Yan, thank you for being a part of the greatest learning experience of my life. I learnt something special from each one of you and I am truly grateful for all the love I got from you guys. You guys made a strange new country feel so much like home.

I would like to express my gratitude towards the Orissa Water Resource Department, especially Mr. Anil Kar for cooperating and facilitating my research by making the requisite data available to me.

Special thanks to my colleagues and friends, Shiwang, Pooja, Suruchi, Kasi and Djaner for their loyal friendship and undying support throughout my course duration. The completion of this thesis is as much your achievement as it is mine.

I would like to sincerely thank anyone who helped me directly or indirectly during this M. Sc. Program whose names I may have missed. Each of your contributions brought me one tiny step closer to my goal and for that I am forever indebted to all of you.

May god bless us, everyone.

TABLE OF CONTENTS

LIST OF FIGURES

LIST OF TABLES

1. INTRODUCTION

1.1 Background

Floods are one of the most frequently occurring, globally pervasive natural hazards which affect millions of people annually (Baldassarre & Schumann, 2011). Developing countries face a greater impact of these due to lower economic resilience and poor management of environmental resources (Koriche, 2012). India has multiple river systems that are frequently flooded due to intense precipitation events during the Indian Summer Monsoons (Shivananda Patro, Chatterjee, Singh, & Raghuwanshi, 2009). The floodplains of these rivers are densely populated and are utilised as agricultural lands and thus flooding events cause high economic losses (Sanyal & Lu, 2005). The Mahanadi River Basin in Odisha is a low lying, paddy growing area that is flooded almost annually (Shivananda Patro et al., 2009). The study reach is a man-made flood diversion channel called Dhanua River, connected to the Kushabhadra River via causeway called Jogisahi escape, located in the Delta region of the Lower Mahanadi Basin.

New techniques for modelling complex floodplain dynamics are urgently required to efficiently mitigate and manage flood events (Hostache et al., 2009). The unavailability of spatially distributed gauge data in developing countries is the greatest obstacle faced while setting up hydrodynamic models (Shivananda Patro et al., 2009). The advent of remote sensing technologies have made it possible to retrieve flood hydrology information from satellite data and use it for calibration and validation of the hydrodynamic model (Guy Schumann, Bates, Horritt, Matgen, & Pappenberger, 2009). However, remote sensing data is ridden with many inherent uncertainties which propagate within the model domain and accumulate in the results (Abebe, Ogden, & Pradhan, 2010).

The differences between the simulated state data and the observed state data arise from a number of sources. These errors tend to progressively increase in magnitude over successive calculation time steps (Alemsged T Haile & Rientjes, 2007). The total error in the results may be attributed to the uncertainty associated with the input data, the forcing data, parameter values, model structure, discretization of the time-space domain and rounding off of values due to computational limitations (Matgen et al., 2004). These uncertainties need to be quantified and reduced wherever possible, such that hydrodynamic modelling with satellite data integration can give more reliable outputs (Hostache et al., 2009).

Synthetic Aperture Radar (SAR) data has proved invaluable for the spatial characterization of floods (Giustarini et al., 2011) due to its all-weather/ all day imaging capability and the low backscatter recorded for water due to specular reflection (Matgen et al., 2010). Two kinds of information can be extracted from SAR images (1) the flood inundation area extent (Di Baldassarre, Schumann, & Bates, 2009) (2) flood inundation depth by integrating with the DEM (Hostache et al., 2006, 2009; Puech, Hostache, Raclot, & Matgen, 2007). The SAR derived flood extent can be effectively used as a calibration target to constrain the model and minimize its prediction uncertainty (Mason, Bates, & Dall' Amico, 2009).

Distributed numerical models are based on the laws of conservation of mass, momentum and energy and solve a specific set of governing equations to predict flood characteristics (Tarekegn, Haile, Rientjes, Reggiani, & Alkema, 2010). On the basis of their approximations of the flow governing equations and the physical complexity of the model, they are classified into 1D and 2D. In principle, 1D models work with the assumption that the water velocity, height and discharge only vary along the channel direction and the lateral flows are negligible whereas 2D models account for both, following the grid layout defined by the DEM geo-reference (Alemsged T Haile & Rientjes, 2007). The hydraulic heads computed at each computational node are intercompared to determine the direction of flow. In 2D hydrodynamic models, while the physical representation of the flood is better, the parameterization of the floodplain roughness coefficient becomes challenging. As the scale of the model gets coarser more land cover types are

encompassed within a pixel, so an average value of the Strickler Manning's Coefficient has to be used which may deviate largely from the actual ground scenario (Alemsged T Haile & Rientjes, 2007). The model setup requires long term field data of discharge/water level as the upstream boundary and at the outlet, free-flow condition is assumed. The target is to calibrate the Manning's coefficient to balance the inflows and out flows in a way that the model reproduces the real world flood inundation area as observed from SAR images. For the purpose of this study, flood inundation maps derived from SAR imagery for historical flood events, will be used for model calibration and validation (Alemseged Tamiru Haile & Rientjes, 2005).

Since, the models have to be approximated over discrete time steps for calculations, they gain some amount of inherent error (Alemsged T Haile & Rientjes, 2007). In combination with the uncertainties in the input remote sensing data, they make the results erroneous which makes quantifying them and reducing them necessary (Di Baldassarre et al., 2009; Mason et al., 2009; Neal et al., 2009; Stephens et al., 2012). The Generalized Likelihood Uncertainty Estimation (GLUE) technique was proposed for quantifying the uncertainties in hydrological modelling (Beven, 1993). GLUE works on the principle of equifinality, i.e. the parameters can have more than one optimal value and the technique has been widely used in hydrology (Aronica, Bates, & Horritt, 2002; Paul D. Bates, Horritt, Aronica, & Beven, 2004; Horritt, 2006).

1.2 Rationale of the Study

Floods destroy 80% of the cropped area and affect thousands in the densely populated Mahanadi River Basin annually, causing severe economic losses (S Patro, Chatterjee, Mohanty, Singh, & Raghuwanshi, 2009). Due to the heavy rainfall in the months of July-September and the gentle relief of the area, the region is frequently plagued by catastrophic floods. The study area was flooded most recently in August, 2014, killing 34 people and destabilising 10 lakh people (Indian Express, Aug 20, 2014). The water logging leads to a cascade of various water borne diseases and are the breeding grounds for filarial, malarial and dengue causing mosquitos which also claim over a dozen lives every year. This emphasizes the need to develop a deeper understanding of the flooding dynamics of the area and the associated uncertainties.

The modelled reach, a man made flood diversion channel, frequently over tops the banks, flooding the surrounding area. Due to the gentle relief, the area also experiences lateral flows during a flood situation which are only accounted for in 2D-hydrodynamic models (S Patro et al., 2009). The average elevation gradient of the area is so low that even rain water doesn't drain out easily. The availability of detailed ground elevation data is also a major constraint faced in 2D- modelling, for this reason, a high resolution DEM was created with ground control points from the field.

There have been limited studies using 2D fully hydrodynamic models in India mainly due to data constraints. This study seeks to calibrate the Manning's coefficient in 1D2D coupled fully hydrodynamic model, MIKE FLOOD, to best represent the flood inundation captured by SAR imagery. This can serve as a kind of pilot study to see if the SAR derived flood extent can be effectively used for model calibration for this study area and if it is found applicable, the technique can subsequently be used for such ungauged basins. This will aid flood management in the area in the future and create healthier living conditions for the inhabitants of the area.

1.3 Objectives and Research Questions

1.3.1 Main Objective

To calibrate a 1D2D-coupled fully hydrodynamic model to best represent the flood inundation area extracted from SAR data and reduce uncertainty for the Mahanadi river delta region.

1.3.2 Sub-Objectives

The specific objectives of the research are as follows:

1. To create a flood inundation from a SAR image of the current flood event minimizing uncertainties.

2. To optimize the DEM for a fully hydrodynamic model.
3. To parameterize the roughness coefficient using a detailed Land Use Map.
4. To validate the simulated results against the SAR derived Flood Extent.

1.3.3 Research Questions

The study will attempt to answer the following research questions.

1. To what extent can the uncertainty, associated with flood extents derived from the SAR images, be reduced in part of the Mahanadi River Delta?
2. How can the DEM be optimized for a fully hydrodynamic model in an area with gentle relief?
3. Which factors influence the parameterization of the roughness coefficient of the flood plain of the Mahanadi Basin?
4. Does the calibrated MIKE FLOOD model simulate the floods effectively for the study area?

1.4 Study Area

1.4.1 Location

The study area is located near the delta region of Mahanadi River lower sub-basin in India. It is located in the north-eastern part of Orissa and lies between the longitudes 85°51'44" E to 85°58'31" E and latitudes 20°16'51" N to 20°8' 53" N (Jaipurkar, 2014). The delta extends over about 6,800 km² of which the study area occupies 953 km². The modelled reach is an artificial flood diversion channel called "Dhanua River" which branches out from the Kushabhadra River through a spillway called "Jogisahi Escape" as shown in figure 1.1. Halfway downstream another causeway at Achyutpur drains water from the Bhargavi River into this channel. The part of the channel before Achyutpur has been modelled in this study. The upstream boundary condition will be applied from Tikarapara and the downstream boundary conditions at Mundali.

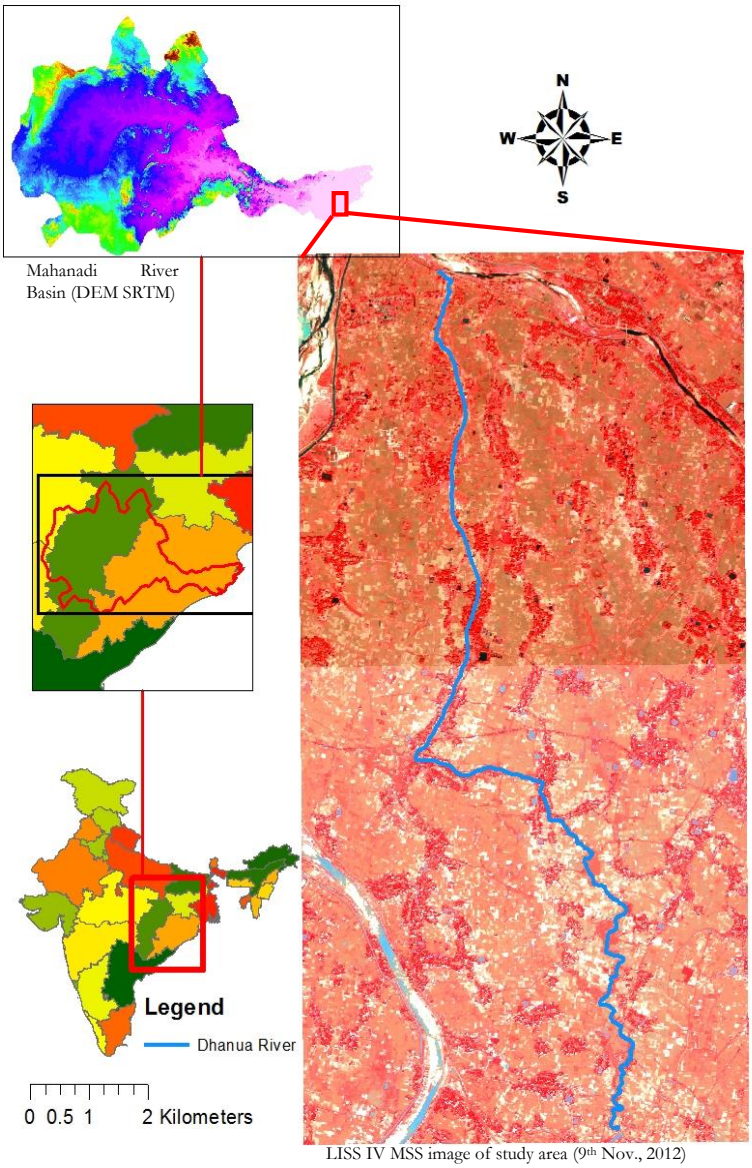

Figure 1.1: Inset map of the study area

1.4.2 Precipitation

The catchment upstream of the delta receives heavy rainfall during the monsoon period causing frequent floods in the rivers Devi, Kushabhadra and Mahanadi. Mahanadi is mainly rain-fed and the water availability undergoes large seasonal fluctuations. Average annual rainfall is 1572 mm, 70% of which is aggregated over the months of June - October during the south-west monsoon (Asokan & Dutta, 2008). Figure 1.2 shows the long term precipitation trend in the study area as reported by the Water Resource Information System of India (WRIS).

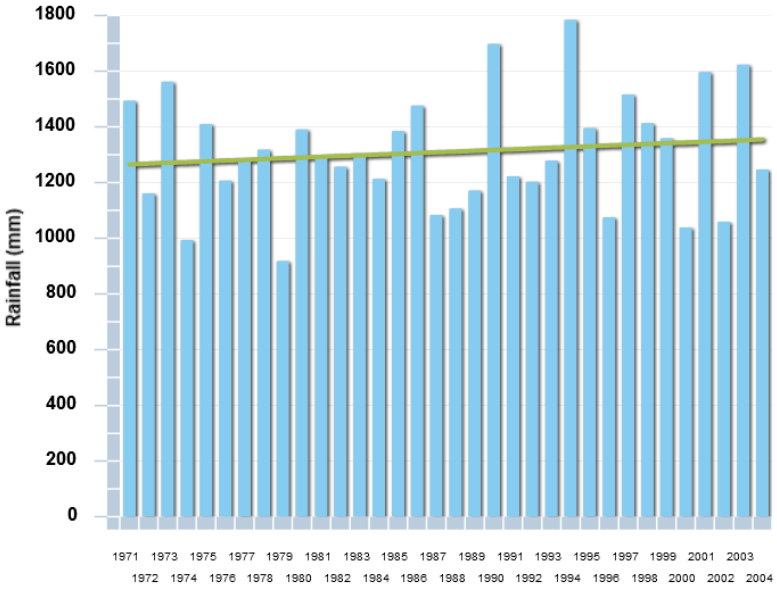

Figure 1.2: Precipitation trends in the Mahanadi River Basin 1974-2004
Source: Water Resource Information System of India (WRIS), Mahanadi Basin Report, 2014

1.4.3 Topography and Land-Use

The downstream part of the catchment is very flat having an average elevation <10m a.m.s.l and a very gentle slope <2% (S Patro et al., 2009). This makes the area very flood prone as rainwater also drains very slowly. The land use of the area is dominated by paddy cultivation. The cropping cycles are such that the lands are barren during the time of the annual flooding in August, the first crop is sown in September. There are some rural settlements in the area, characterized by the surrounding vegetation. Figure 1.3 is a field photograph depicting the chief land-use of the study area and figure 1.4 shows the make shift *kachha* houses that the natives of the area live in. These houses have to be rebuilt after each flood event. Figure 1.5 depicts the land use land cover map of the watershed containing the study reach, a part of the lower Mahanadi Basin.

Figure 1.3: Paddy fields in the study area

Figure 1.4: Rural settlements - Mud Houses

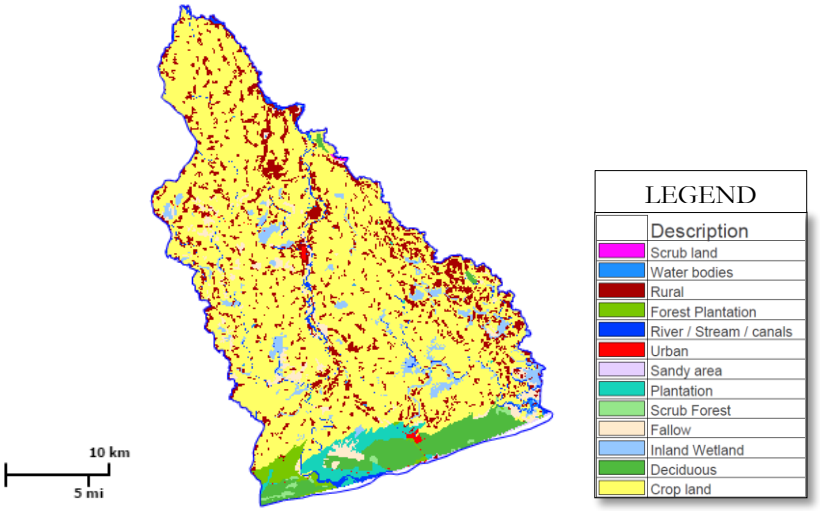

Figure 1.5: Land use map of the watershed containing the study reach
Source: WRIS, 2015.

1.4.4 Drainage

The study area has an extensive irrigation canal network, as agriculture is the chief occupation and land use. They maybe one of the reasons for such widespread flooding in the area as well as none of them have levees constructed and can easily be breached by a flood wave. Hirakud Dam is the biggest hydropower project in the area at 347.5 MW but it was mainly built for flood control purposes. Figure 1.6 illustrates the extensive irrigation canal network in the study area. Figure 1.7 shows field photographs of the DGPS Survey and the fish capturing nets at the Jogisahi Escape.

Figure 1.7: Field photographs

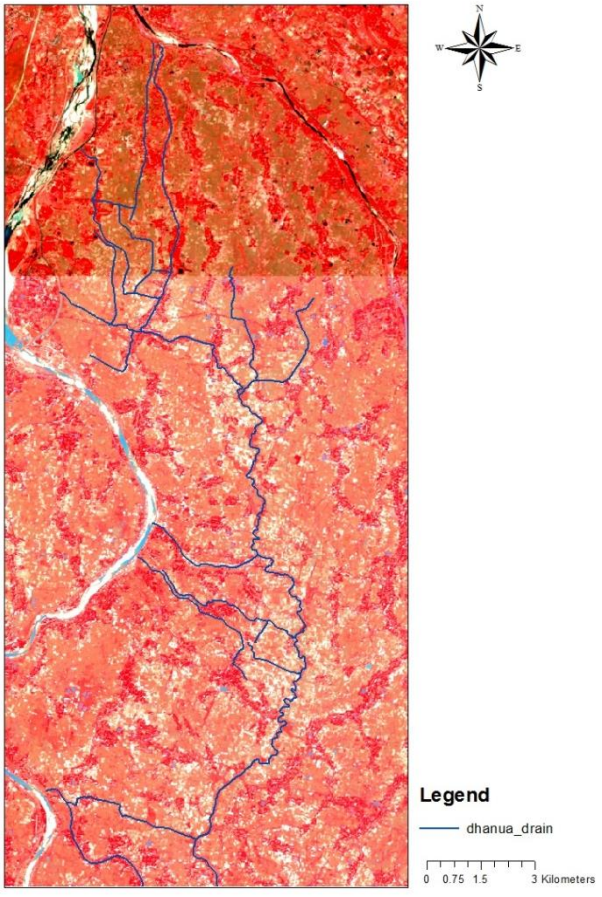

Figure 1.6: Drainage map of the study area

1.5 Thesis Outline

The outline of this thesis report consists of five chapters. The first chapter includes the introduction, objectives, research questions and a description of the study area. The second chapter summarizes the state of the art in the available literature relevant to the study. The third chapter elaborates the methodology employed, the reasons of choosing them and a review of the advantages and disadvantages. Choice of data and their pre-processing techniques are also discussed at length. The fourth chapter describes the results and discusses them. The fifth chapter presents some conclusions drawn from the study and some recommendations for future research.

2. LITERATURE REVIEW

2.1 Flood Extent Delineation

Flood extent delineation has been fascinated researchers ever since the advent of aerial photography which afforded a synoptic view of affected areas. This was followed by the transition to optical satellite imagery, followed by Synthetic Aperture Radar (Paul D. Bates, 2012). Over the years, many techniques such as visual interpretation, image histogram thresholding, automatic classification alorithms such as active contours (snake), texture based classification algorithms, multi temporal change detection, etc have been developed which have been extensively reviewed by Sanyal & Lu, in 2004 and Schumann et al., in 2009. However, the superiority of one of the aforementioned techniques over another has not been established so far.

In this study, SAR images have been chosen to demarcate the flood extent as they have all day and all weather imaging capabilities (Hostache et al., 2009) which is especially important for flood inundation studies as cloud cover is a major obstacle for the use of optical data. The low backscatter given by water due to specular reflection of the incident microwave beam is also an added advantage as it affords easy identification of flooded pixels (Hostache et al., 2006). The use of SAR data has to overcome other challenges like detecting floods under vegetated areas where the canopy causes volume scattering (M. S. Horritt, 2000). Another hindrance is the high sensitivity of microwave data to surface roughness which increases the backscatter. This essentially signifies that if the wind speed is high in a flooded area, it creates ripples on the water surface, increasing backscatter and detecting the flooded area accurately becomes trickier (M.S. Horritt, 2006).

Moreover, in the boundary region as the transition happens from flooded to non-flooded pixels the radar backscatter increases gradually, thus making the identification of a sharp flood extent boundary nearly impossible (Matgen et al., 2004). This introduces some uncertainties in the flood extent detection from SAR as the choice of the threshold value for the backscatter can be rather subjective . Over time various techniques have been developed for efficient flood extent mapping such as radiometric thresholding (Hostache et al., 2006), image texture classification, active contour algorithm, etc. which were compared by Di Baldassarre et al., in 2009. More recently, their application to derive water levels in combination with a high resolution DEM was explored by many researchers (Giustarini et al., 2011; Hostache et al., 2006, 2009; Hostache, Lai, Monnier, & Puech, 2010; Montanari et al., 2009). The water levels were seen to be important for vulnerability analysis, danger warnings as well as damage assessment (Hostache et al., 2006). They were derived using the assumption of hydraulic coherence that for low flows the water level decreases from upstream to downstream and the model was validated against these spatially distributed values (Hostache et al., 2009). Until recently the model parameterization was done mainly via batch calibration which assumes a time invariant nature of the parameter values, using Data Assimilation techniques the parameters are recalibrated during the model run at each time step (Moradkhani, Hsu, Gupta, & Sorooshian, 2005). This technique is still in its infancy in the field of hydrodynamic modelling but there have been some studies using conceptual hydrological models (Dimet, Castaings, Ngnepieba, & Vieux, 2009; Giustarini et al., 2011; Noh, Tachikawa, Shiiba, & Kim, 2013; Slivinski, Spiller, & Apte, 2015).

Several techniques have been chosen for flood delineation due to the subjectivity in choosing one over the other. Radiometric thresholding was one of them (Hostache et al., 2009) as it also accounts for some of the subjectivity in the thresholding. In this technique two thresholds are used in place of one, thus dividing the images into certainly flooded, non-flooded and potentially flooded pixels. The potentially flooded pixels are then checked against optical images of comparable dates and resolutions. The pixels where the presence of flooding remains uncertain after such analysis, are dropped from the calibration target and are considered as NoData pixels and thus, the uncertainty associated with them is successfully removed from the model domain. The advantage is that it is a really fast and easy method to create flood

maps, as opposed to the more tedious as well as computationally intensive texture analysis (Guy Schumann, Di Baldassarre, & Bates, 2009). The disadvantage of such an approach is it's reliance on visual interpretation which makes it lose objectivity. The process of checking and removing each uncertain pixel is also tedious and labour intensive (Di Baldassarre et al., 2009). Texture based classification was also used to create flood maps from the same SAR image. The filters used were mean euclidean distance and variance. The last method used was visual interpretation. The maps thus obtained were thus combined to generate the possibility of inundation map, which was then used for calibration (Mason et al., 2009).

2.2 The Role of Topographic Data

Topographic or terrain data represented in the form of a Digital Elevetation Model (DEM) serves as the physical representation of the channel bathymetry and the flood plain geometry (Tarekegn et al., 2010). The dearth of geometrically accurate cross-sectional data often leads to a flawed depiction of the hydraulic conveyance factor which contributes to the uncertainty in the simulated flood dynamics (Tarekegn et al., 2010). Most of the outputs of hydrodynamic models such as water stages, discharge and flood extent are dependent on DEM derived variables such as slope, aspect, flow direction, etc. (Tarekegn, 2009a). It is thus, imperative to represent the topographical information as accurately as possible, as 2D model results are almost completely reliant on it. Coarser resolution causes an averaging of the topographic features and finer characteristics like dykes are rendered indiscernible by the model, which may reflect n the flow characterisctics described by the model.

Guy Schumann, Pappenberger, & Matgen, in 2008, concluded that usable water stages could be derived from LiDAR, topographic contours and the global SRTM DEM, the in descending order of accuracy. The effect of DEM resolution (1.5m – 15m using LiDAR) on 2D-hydrodynamic models was studied by Alemseged Tamiru Haile & Rientjes, in 2005, showing that the optimal grid size for modelling was 10m after which making the resolution finer has no significant impact on the results. Wu, Li, & Huang, in 2008, conducted a similar study where they used USGS DEMs from 10 – 200 m resolutions and compared the outputs, tested by many others in different study areas (Li & Wong, 2010; Sanders, 2007). Tarekegn et al., 2010, assessed the potential of an ASTER generated DEM (15m) for 2D-Hydrodynamic Modelling for the Ribb River in the Lake Tana Catchment in Ethiopia. They tested a technique of linear interpolation to derive the channel bathymetry, between points of known elevation, using the Inverse Distance Weighting where they found the weighting factor of 4 to be ideal for such applications. In 2012, a new algorithm was proposed to correct the SRTM DEM (90m) using flow direction maps from HyrdoSHEDS, rendering it useful for Hydrodynamic modelling tested using LISFLOOD-FP (Yamazaki et al., 2012).

The appropriate DEM resolution must be chosen carefully as each grid cell is also a computational cell. There is a trade off between the simulation time and the accurate representation of topography. An optimum resolution needs to be used which gives a reasonably precise illustration of the flood plain topography and at the same time doesn't increase the simulation time significantly (Sanders, 2007). Larger grid sizes mean loss of important information which affect flood propagation due to averaging and the average value may deviate greatly from the actual on-ground scenario (Alemseged Tamiru Haile & Rientjes, 2005). There is a dire need of explaining the effects this has on model performance and the reliability of simulation results.

2.3 Hydrodynamic Flood Modelling

2.3.1 Overview

The recent developments in hydrodynamic modelling can be attributed to two factors chiefly, the capability of capturing high resolution and accurate topographic data such as LiDAR (accuracy up to ± 15 cm) and the progress in numerical and computational efficiency (Hunter, Bates, Horritt, & Wilson, 2007). Earlier the models were solving the Kinematic or Diffusion Wave approximations to achieve a physical representation of the flood in the model domain as solving the full set of St. Venant shallow

water equations was too computationally intensive. These cannot fully account for the physical complexities and the transient characteristics of channel flow in the model domain which is of utmost importance (Tarekegn, 2009a). Newer, numerical engines can solve the full set of shallow water equations without losing too much computational time even with high resolution digital elevation models (Paul D. Bates, 2012).

2.3.2 Modelling Approaches

There are several ways to approach flood modelling. They have been listed here in increasing order of complexity (P D Bates & De Roo, 2000).

2.3.2.1 Planar Water Surface Approach

The maximum flood water level recorded by the gauge is assumed to be a planar surface and is overlain on the underlying raster or TIN based DEM and all areas below this surface are assumed to be flooded. No channel or floodplain routing is applied to the flood wave (Priestnall, Jaafar, & Duncan, 2000).

2.3.2.2 Storage Cell Approaches

The storage cell approaches are diverse and of varying complexities.The simplest one uses uniform flow formulae using the designated channel cells (P D Bates & De Roo, 2000) and the discretisation is minimal, the channel and the left and right floodplains are represented by single cells (Cunge, Holly Jr., & Verwey, 1976). A slightly more complex variation of this approach is using multiple polygonal cells following the natural boundary, linked by the channel, for floodplain representation (Estrela, 1994). Bechteler, Hartmaan, & Otto, 1994, added 1D channel routing to this and characterised the flood plains using TIN cell faces (FLOODSIM). Lastly, a 1D kinematic wave, solved using an explicit finite difference procedure for the channel routing was proposed by P D Bates & De Roo, 2000. They used a uniform flow routing for the floodplains and a raster based discretisation derived from the DEM (LISFLOOD-FP).

2.3.2.3 Hydrodynamic Models

Fully hydrodynamic models are those which solve the complete set of Saint Venant shallow water equations based on the conservation of mass and momentum (M S Horritt & Bates, 2002). One dimensional models (1D) assume that the flow of water is only transient along the direction of channel flow and lateral and depth components of the flow field vectors are ignored (Alemseged Tamiru Haile, 2005). The model domain is discretised as a series of transversal cross sections, perpendicular to the flow direction and the governing equations are solved at each of these. The geometry is assumed to vary linearly or constant between two subsequent cross sections. While such an approach is computationally efficient, it fails to depict the floodplain dynamics as the representation is not in the form of a surface but isolated cross-sections (M S Horritt & Bates, 2002; Hunter et al., 2007). 1D models lack the potential to accurately represent the complex physical characteristics of the flood, leading to the proliferation of 2D, 1D2D and 3D models (Alemseged Tamiru Haile & Rientjes, 2005; Tarekegn et al., 2010).

Two dimensional models (2D) consider transient flow characteristics in both the longitudinal and transverse directions and solve the 2D St. Venant Equations with turbulence closure (P D Bates & De Roo, 2000). As the heterogeneity of the floodplains increases, their depiction in the model domain becomes tougher as does the parameterisation of the roughness coefficient (Alemsged T Haile & Rientjes, 2007). The quality of 2D modelling and the reliability of its results is greatly dependant on obtaining high resolution topographic data which accurately represents the bathymetry of the channel (Li & Wong, 2010). 2D models are discretised in the form of structured grids (finite difference method) or unstructured grids (finite volume and finite element methods) usually in the form of triangles or quadrilaterals (P D Bates & De Roo, 2000). 2D models also have heavy computational demands depending on the grid size (Carrivick, 2006). If a larger grid size is used, the floodplain features are lost and an average value has to be chosen for the cell which may deviate largely from the ground scenario

(Werner, Hunter, & Bates, 2005). Conversely, while a fine resolution computational grid allows for efficient parameterisation of the surface roughness, it increases the computational time exponentially (G. Schumann et al., 2007). Keeping this trade off in mind an optimal resolution must be chosen.

1D2D coupled models address most of the disadvantages of the standalone versions. The combined models represent the channel flow in 1D which is a fair assumption as within channel transverse flows can be considered to be negligible, especially during a flood situation and the floodplain is modelled in 2D (Alemseged Tamiru Haile & Rientjes, 2005).

2.3.3 Solution Approaches

The St. Venant equations are a set of continuous partial differential equations which can only be solved using numerical methods (Tarekegn, 2009a). They are solved by iteratively computing, continuously varying differential terms, at discrete points in space and time, giving approximate solutions. Commonly used approaches for this space domain discretisation. The linearizing of the continuous differential equations can be achieved using the Finite Difference Method (FDM), Finite Element Method (FEM) or the Finite Volume Method (FVM). While FVM is better at capturing discontinuities, FEM divides the solution domain into a number of smaller sub-regions solving for each region separately (finite elements) and requires interpolation polynomials to illustrate the distribution on the dependant variables over the elements (Alemseged Tamiru Haile, 2005).

The MIKE engine uses the Finite Difference method to convert the St. Venant Shallow Water equations into a rectangular computational grid or mesh consisting of h and Q points approximated over discrete finite increments in both space and time. Such discretization and approximations introduce an error in the system directly proportional to the size of the grid cells. The equations $\frac{\partial h}{\partial x}$ and $\frac{\partial h}{\partial t}$ have been approximated using the finite difference approach as under:

$\frac{\partial h}{\partial x} \approx \frac{{h_{i+1}}^t - {h_i}^t}{\Delta x}$, forward discretisation in space,

$\frac{\partial h}{\partial t} \approx \frac{{h_i}^{t+1} - {h_i}^t}{\Delta t}$, forward discretisation in time;

where h= water level, x=distance from the origin in the x-direction and t= time.

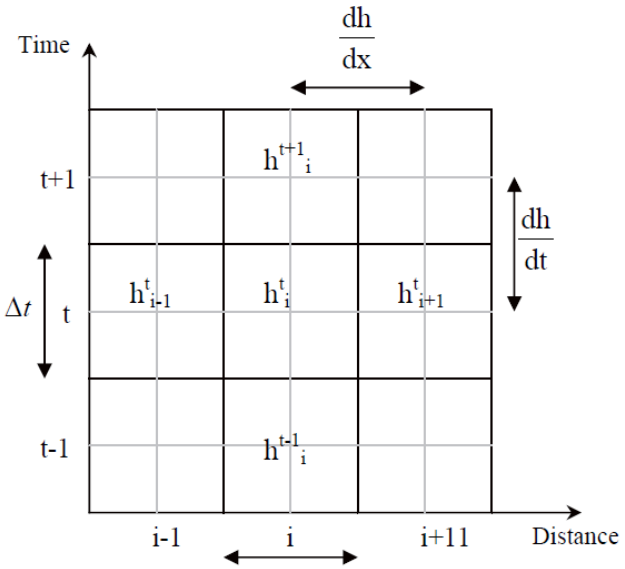

Figure 2.1: Graphical representation of the time space domain discretisation (Tarekegn, 2009).

2.3.4 Initial and Boundary Conditions

Initial conditions are the states of the system being modelled at t= 0 and before that. They define the starting point for the trajectory of changes observed in the system properties over the simulation period (DeChant, 2014). Boundary conditions specify the influence of universal processes on the model domain, i.e. the physical constraints placed on the model states and processes (Tarekegn et al., 2010). Initial conditions can be derived from an a priori knowledge of the system, from gauge data or from a pre simulation warm-up period model run. Boundary conditions are usually defined by a time series of hydrometric data such as an inflow hydrograph. Mathematically, they can be of three types: Dirichlet condition (specified head boundary), Neumann condition (specified flow boundary) and Cauchy condition (head-dependant flow boundary) (Alemseged Tamiru Haile & Rientjes, 2005).

2.4 Model Cal/Val and Sensitivity Analysis

The disparity between the model simulated scenarios and observed ones for the same time frame need to be brought within an acceptable limit of allowable deviations (Alemseged Tamiru Haile & Rientjes, 2005). This can be achieved by calibrating the model. The model parameters are seldom attached to unique values which give ideal results. Parameters usually vary over a range of acceptable values and have to be fine-tuned according to the specific problem situation the model is being applied to (Stephens, Bates, Freer, & Mason, 2012). Depending on how sensitive the model is to each of these parameters a change can be observed in the outputs, which can then be manipulated to give a best fit. This can be accomplished by conducting a sensitivity analysis, which can be of two types; model sensitivity analysis - tests the response of the model to extreme forcing and parameter sensitivity analysis – tests the impact of a change in the parameter values on the results (Rientjes et al., 2011). Hydrodynamic models have been found to be sensitive to the physical model parameters i.e. DEM resolution and surface roughness (Carrivick, 2006; Merwade, Cook, & Coonrod, 2008; Alemsged T Haile & Rientjes, n.d.; Jung et al., 2012; Mani, Chatterjee, & Kumar, 2013). Finally, the model has to be tested for its predictive capability by using records out of the calibration period which give an unbiased view of the model performance (Hunter et al., 2007).

The output dataset we want the model to mimic is called the calibration target. Flood inundation studies use flood extent maps/satellite imagery, distributed field observations of the flood and hydrometric data from river gauges (Gumindoga, Rwasoka, & Murwira, 2011). The primary concern of any flood inundation study is the extent, depth and duration, as these factors would determine the vulnerability of the affected areas. Another concern is the unavailability of gauge data at the outlet which is often the reason why floods in ungauged basins can't be modelled (Shivananda Patro et al., 2009). This is a huge limitation as the areas which most direly require flood management interventions are in acutely data deficient environments, mostly developing countries (Koriche, 2012). Experts have argued the appropriateness of validating spatial 2D results with point data. The reason behind investing more computational time in 2D models is to model efficiently the complex floodplain flow processes, which are not represented adequately by the point discharge data (Baldassarre & Schumann, 2011).

This study proposes to use an approach proposed by Di Baldassarre et al., in 2009, to calibrate hydrodynamic models using uncertain satellite data of flood extent. The delineation of flood boundaries from SAR data have known to be fairly ambiguous due to the contribution of surface roughness and the transient characteristics of the boundary region (Baldassarre & Schumann, 2011; Paul D. Bates, 2012; Guy Schumann, Bates, et al., 2009). Several methods of flood limits extraction from SAR data have been used historically such as visual interpretation, texture based analysis, histogram thresholding, etc. However, the subjectivity in the choice of the flood outlining approach is unavoidable. However, this uncertainty can be dealt with using a possibility of inundation map (POI) which takes in to account an ensemble of flood maps created using all of the different methods and gives as an output the values of the possibility of flooding of each pixel (Guy Schumann, Di Baldassarre, et al., 2009).

2.5 Model Selection

Selection of an appropriate modelling tool for a given study area is dependent on many factors and can only be determined with a combination of a priori knowledge of the field and expertise. The major factors that should contribute to this decision-making process are the model outputs we require, the availability of input data, the model structure, model performance on a site similar to the study area and finally, the price and the availability of the model (Koriche, 2012). Different modelling tools are available both commercially and as open source packages. The most widely used 1D models are HEC-RAS, FLDWAV, FLUCOMP, SOBEK, MIKE 11, etc.; 2D models such as MIKE 21, TELEMAC – 2D, DELFT-3D, DELFT-RMS, KALYPSO; and 1D2D coupled models are MIKE FLOOD, SOBEK, LISFLOOD-FP, etc.

As 1D2D coupled models have proven more advantageous over either standalone model, they dominate the modelling scenario today. While 2D models with the right DEM resolution can give exemplary

results, they are very computationally intensive and such high resolution topographic data is rarely accessible (S Patro et al., 2009). In this particular study the model MIKE FLOOD was chosen based on its availability and the strong computing capabilities of the backend model engine. Several studies have shown the model's capability to run relatively faster than other proprietary models (Chatterjee, Forster, & Bronstert, 2008). The model stores the values of maximum water depth and the flux for each pixel at each time step (Vanderkimpen, Melger, & Peeters, 2009). The MIKE 11 engine which handles the channel flow in 1D is also capable of changing the standard flow equations to an alternative set which uses a single expression for both flow regimes and applies an empirical reduction coefficient as soon as the downstream energy head exceeds the water level at the breach crest (Vanderkimpen et al., 2009).

2.6 Uncertainties in Hydrodynamic Models

Hydrodynamic modelling is ridden with some inherent uncertainties associated with the model structure and input remote sensing data which need to be dealt with. These propagate and accumulate over the simulation results. This makes quantifying them and reducing them necessary (Di Baldassarre et al., 2009; Mason et al., 2009; Neal et al., 2009; Stephens et al., 2012). The disparity between model calculated state outputs (V_{sim}) and observed real world state data (V_{obs}) arises due to the following errors which could be either positive or negative (Alemsged T Haile & Rientjes, 2007):

- Random or systematic errors in the forcing data (ε_i), e.g. precipitation data
- Random or systematic errors in the recorded state data (ε_r), e.g. water levels
- Errors due to non-optimal parameter values (ε_{no})
- Errors due to incomplete or biased model structure (ε_s)
- Errors due to the time space model domain discretization (ε_d)
- Errors due to rounding off (ε_{ro})

Hence the total simulation error is given by the following relation:

$$V_{obs}\text{-}V_{sim} = \varepsilon_t = \varepsilon_i + \varepsilon_r + \varepsilon_{no} + \varepsilon_s + \varepsilon_d + \varepsilon_{ro} \quad \textit{Equation 2-1}$$

Over the last few decades, much progress has been made in addressing the issues of uncertainty (Guy Schumann, Bates, et al., 2009). Several statistical approaches have been developed to quantify them, such as the Generalized Likelihood Uncertainty Estimation techniques (Beven & Binley, 1992). Several variations of the GLUE have been developed and successfully used since (Paul D. Bates, Horritt, Aronica, & Beven, 2004). In 2005, a technique for analysing the uncertainty in the unsteady flow component (UNET) for the 1D-hydrodynamic model HEC-RAS using GLUE, by taking into account the ability of effective extreme parameters and real physical reach roughness values to perform equally well, was presented (Pappenberger, Beven, Horritt, & Blazkova, 2005). Guy Schumann et al., in 2008, assessed the uncertainties associated with the water stages derived from a single SAR image using an extended GLUE approach. In 2006, Horritt validated a simple cellular flow model LISFLOOD-FP, using reliability diagrams and the RMSE between uncertain predicted inundation and observed proportion of flooding, calibrating within the GLUE framework. The GLUE approach while efficient, is really costly in terms of computational time, as a single glue ensemble requires tens of thousands of simulations. An alternate approach to quantify the uncertainty is to observe the standard deviations of parameter sets in a smaller, scientifically reasonable ensemble of simulations. (M. S. Horritt, 2000).

2.7 Previous Studies on the Mahanadi River Basin

The Mahanadi River Basin has widely been studied due to the dense natural drainage as well as irrigation networks in the area and the tendency of floods occurring every monsoon season. A study was conducted in 2008, to assess the status of water resources of the Mahanadi basin under projected climate change scenarios as predicted by CGCM2 (Canadian Centre for Climate Modelling and Analysis General Circulation Model). The forecasted precipitation was given to a physically based distributed hydrologic model (DHM) which prophesied a 38% increase in peak runoff values for September, 2075-2100 and a 32.5% decrease in lean flow during April, 2050-75, implying that the region will experience increasingly

intense flood and drought events annually (Asokan & Dutta, 2008). This study emphasized the need to further scrutinise the flood management strategies in the area. The flooding for the river Mahanadi was modelled for the years 2001-2002 using an STRM DEM and surveyed cross-sections in MIKE FLOOD and validated against hydrometric data as well as a WiFS field image of the actual flood for the 2004 event (S Patro et al., 2009; Shivananda Patro et al., 2009).

The particular flood diversion channel selected for this study, Dhanua River, has rarely been studied in the past but it is responsible for severe flooding almost annually, thus making this research imperative. Previously, there has been a study on this channel using LISFLOOD-FP and the freely available online DEMs, in which SRTM reportedly gave the best results (Jaipurkar, 2014; S. K. Singh, 2004).

3. MATERIALS AND METHODS

3.1 Conceptual Framework

A coupled 1D2D – fully hydrodynamic model was used to simulate a channel flood in the Dhanua River, located in the delta region of the Mahanadi River Basin, calibrated and validated using SAR based flood maps of the events. At the upstream boundary condition an inflow hydrograph was provided and at the downstream boundary, hydraulic free flow condition was assumed. CARTOSAT – I, stereo pair of images (2.5 m), supplemented with ground surveyed DGPS readings, were used to create a high resolution DEM from which cross-sections and floodplain topography was derived. A detailed land-use land cover map was created from a LISS IV multispectral image (5.8 m) to appropriately characterize the surface roughness coefficient.

Hydrodynamic models use some practical assumptions which compromise the model's ability to simulate some of the more complex real world phenomena. The underlying assumptions of MIKE FLOOD are listed below (DHI, 2014c):

- The water is incompressible and homogeneous, i.e. negligible variation in density.
- The bottom-slope is small, thus the cosine of the angle it makes with the horizontal may be taken as 1.
- The wave lengths are large compared to the water depth. This ensures that the flow everywhere can be regarded as having a direction parallel to the channel bottom.
- To the bottom, i.e. vertical accelerations can be neglected and a hydrostatic pressure variation along the vertical can be assumed.
- The exchange of momentum between the channel and the floodplain is ignored.
- The flow is subcritical.

Major software packages used in this study are ArcGIS 10.1, ERDAS Imagine 2014, ENVI 5.0, SARScape, LPS 2011, HEC-GeoRAS, HEC-RAS, MIKE 11, MIKE 21 and MIKE FLOOD. Figure 3.1 describes the work flow of the project.

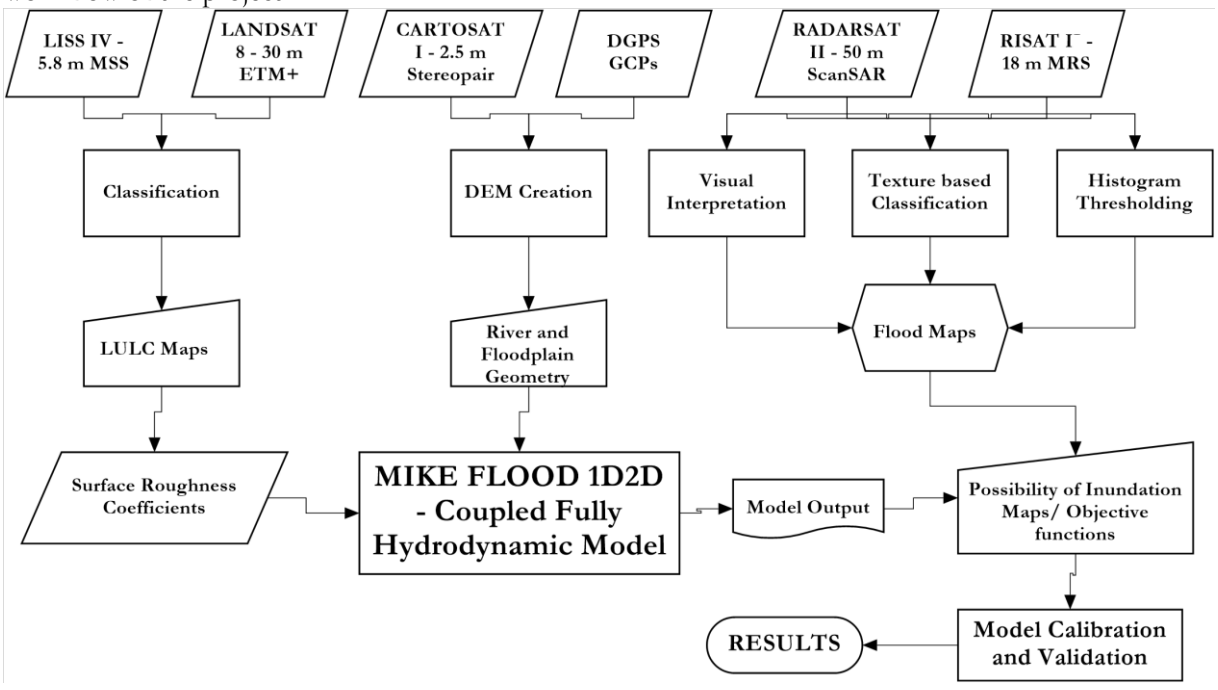

Figure 3.1: Conceptual Framework of the Project

3.2 Model Approach

MIKE FLOOD is a coupled hydrodynamic flood model developed by the Danish Hydraulics Institute (DHI), which integrates the one-dimensional models MIKE URBAN (MOUSE), MIKE 11 and the two-dimensional model MIKE 21 into a single, dynamically coupled modelling system. MIKE FLOOD simulates the inundation by solving the full St. Venant's Shallow Water equations but the user can choose the Kinematic or Diffusive Wave (Zero Inertia) approximations as well. The model domain of MIKE 11, each cross section is spatially discretised into staggered 3D rectangular grids (DHI, 2014c).

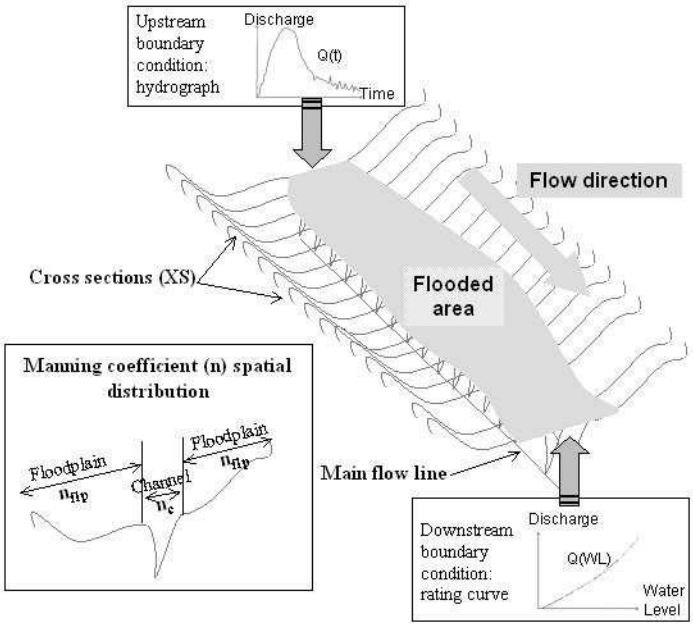

Figure 3.3: One Dimensional model geometry and the channel roughness coefficients (Hostache et al., 2009)

As shown in figure 3.3 the setup of a hydrodynamic model requires the knowledge of the three dimensional geometry of the flood plain and the channel, initial and boundary conditions and hydraulic parameters (Hostache et al., 2009). For 1D models such as MIKE 11, the stream centreline has to be outlined and cross sections positioned perpendicular to it. It must be ensured that the cross sections are perpendicular to the direction of flow and do not intersect the channel twice or each other. This may result in disturbing the hydraulic conveyance through the channel.

The MIKE 21 model is capable of handling flooding and drying, spatially varying surface roughness, eddy viscosity, Coriolis forces and wind friction. The hydraulic head is calculated at the centre of each grid cell and compared in the four neighbouring directions to determine the final direction of flow (Moore, 2011).

This study utilizes the combination of MIKE 11 and 21 which can be connected using various types of links provided in MIKE FLOOD such as a standard link, structural link (weir, culvert, etc.), lateral links, etc. The standard links are explicit and are used to link the ends of a MIKE 11 branch to the 2D computational mesh of MIKE 21 where the boundary conditions can be supplied as rating curves (DHI, 2014). The discharge contributed by MIKE 11 affects the continuity and momentum equations of MIKE 21. Lateral links are explicit too and allow the lateral flow of water from the MIKE 11 branch to the 2D computational mesh of MIKE 21. As 1D models do not consider cross channel flows, momentum cannot be conserved across such a link (Gilles & Moore, 2010). Figure 3.4 illustrates the nature of various linkages available in MIKE FLOOD.

3.2.1 Model Equations

MIKE 11 uses the complete set of Saint Venant Equations to simulate flow in a channel. Illustrated below are the equations used:

The equation of continuity for 1D channel flow is given by;

$$\frac{\partial Q}{\partial x} + \frac{\partial A}{\partial t} = q \quad \text{.....Equation 3-1}$$

And the equation of momentum by; $\frac{\partial Q}{\partial t} + \frac{\partial \left(\alpha \frac{Q^2}{A}\right)}{\partial x} + gA\frac{\partial h}{\partial x} + \frac{gQ|Q|}{C^2AR} = 0$..... *Equation 3-2.*

Where,

Q	discharge
A	flow area
q	lateral inflow
h	stage above datum
C	Chezy resistance coefficient
R	hydraulic or resistance radius
α	momentum distribution coefficient

The first term addresses the local acceleration; the second describes convection acceleration; the third represents the water level gradient; the fourth and fifth are the bed and wind friction terms respectively (Alemsged, 2005).

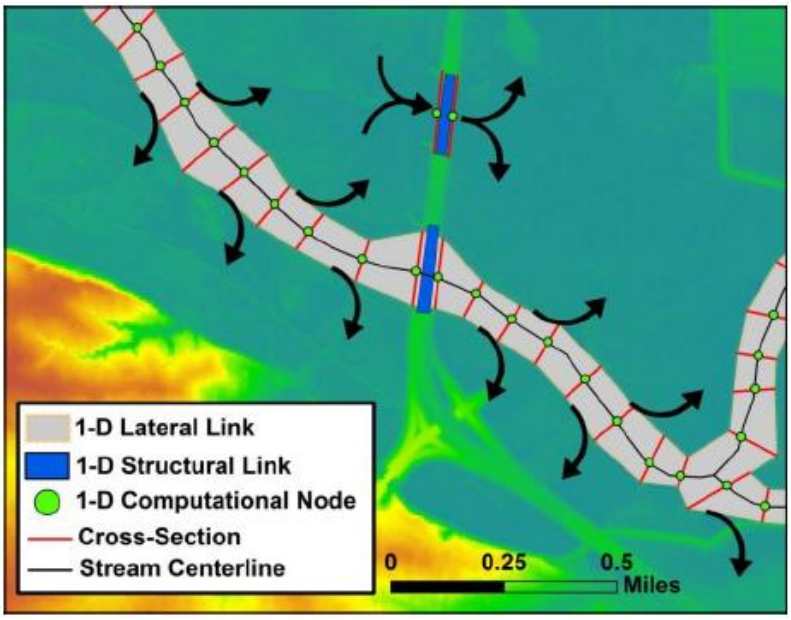

Figure 3.4: Linkages between MIKE 11 and the 2D computational mesh of MIKE 21 (Gilles & Moore, 2010)

MIKE 21 uses the following equations of continuity and momentum to simulate overland flows, following the laws of conservation of mass and momentum.

$$\frac{\partial \xi}{\partial t} + \frac{\partial p}{\partial x} + \frac{\partial q}{\partial y} = \frac{\partial d}{\partial t} \quad \text{.....Equation 3-3}$$

$$\frac{\partial p}{\partial t} + \frac{\partial}{\partial x}\left(\frac{p^2}{h}\right) + \frac{\partial}{\partial y}\left(\frac{pq}{h}\right) + gh\frac{\partial \xi}{\partial x} + \frac{gp\sqrt{p^2+q^2}}{C^2.h^2} - \frac{1}{\rho_w}\left[\frac{\partial}{\partial x}(h\tau_{xx}) + \frac{\partial}{\partial y}(h\tau_{xy})\right] - \Omega_q - fVV_x + \frac{h}{\rho_w}\frac{\partial}{\partial x}(p_a) = 0 \quad \text{.....Equation 3-4}$$

$$\frac{\partial q}{\partial t} + \frac{\partial}{\partial x}\left(\frac{q^2}{h}\right) + \frac{\partial}{\partial y}\left(\frac{pq}{h}\right) + gh\frac{\partial \xi}{\partial y} + \frac{gq\sqrt{p^2+q^2}}{C^2.h^2} - \frac{1}{\rho_w}\left[\frac{\partial}{\partial y}(h\tau_{yy}) + \frac{\partial}{\partial x}(h\tau_{xy})\right] + \Omega_p - fVV_y + \frac{h}{\rho_w}\frac{\partial}{\partial y}(p_a) = 0 \quad \text{.....Equation 3-5}$$

Where the symbols stand for the following:

h(x,y,t)	water depth (m)
d(x,y,t)	time varying water depth (m)
ξ(x,y,t)	surface elevation (m)
p.q(x,y,t)	flux densities in x- and y-directions ($m^3/s/m$)=(uh,vh); (u,v)=depth averaged velocities in x- and y-directions
C(x,y)	Chezy resistance ($m^{1/2}/s$)
g	acceleration due to gravity (m/s^2)
f(V)	wind friction factor
$V,V_x,V_y(x,y,t)$	wind speed and components in x- and y-directions (m/s)
Ω(x,y)	Coriolis parameter, latitude dependent (s^{-1})
$P_a(x,y,t)$	atmospheric pressure ($kg/m/s^2$)
ϱ_w	density of water (kg/m^3)
x,y	space coordinates (m)
t	time (s)
$\tau_{xx}, \tau_{xy}, \tau_{yy}$	Components of effective shear stress

The terms in the momentum equation represent the physical processes that govern flow momentum in the real world, such as pressure, change in velocity and friction due to shear stress. In MIKE FLOOD, the floodplain cells are inundated in response to channel flow, based on relative water depths (M S Horritt & Bates, 2002). Such an approach ignores effects such as; momentum transfer between the channel and the floodplain; effects of advection and secondary circulation on mass transfer. The alternating direction implicit (ADI) technique is used in MIKE 21 HD for the integration of the equations pertaining to the conservation of mass and momentum in the space-time domain (Euskal, Agencia, & Ura, 2003). Each of the equation matrices for every direction in each grid is solved using a Double Sweep algorithm (Mani et al., 2013).

3.2.2 1D2D – Coupling in MIKE FLOOD

The 1D river model MIKE 11 can be linked via a lateral boundary to the MIKE 21 grid. The flow through this link is dependent upon a structure equation mostly weir, which represents the over topping of a river bank or levee and the respective water levels in MIKE 11 and MIKE 21. The geometry of the structure can be determined from cross section bank markers, MIKE 21 topographical levels, a combination of the highest of each, or from an external file. The flow through a lateral link is distributed into several MIKE 11 *h* points and several MIKE 21 cells/elements.

The geometry of the structure is subdivided into a series of internal structures to utilise all of the available information. Each internal structure has a bed level and width determined from the resolution of points defined along the structure. Each internal structure is assigned a water level from the river and from the overland solver during computation, which is calculated by interpolating levels at existing calculation points onto the internal structures as illustrated in figure 3.5.

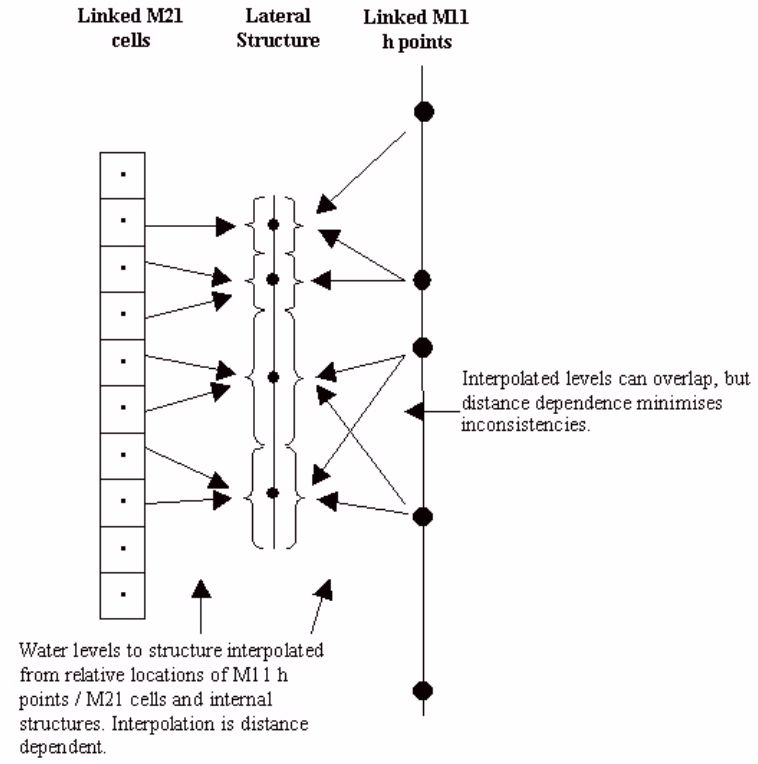

Figure 3.5: Lateral Links - Interpolation of water levels
Source: MIKE FLOOD User Manual, DHI, 2014.

A standard structure equation (weir equation – MIKE 11) is used to compute the flow across each internal structure, using the calculated width, bed level and interpolated water levels. The flow from each internal structure is then distributed to/from the MIKE 11 h points and MIKE 21 cells as shown in figure 3.6 (DHI, 2014b).

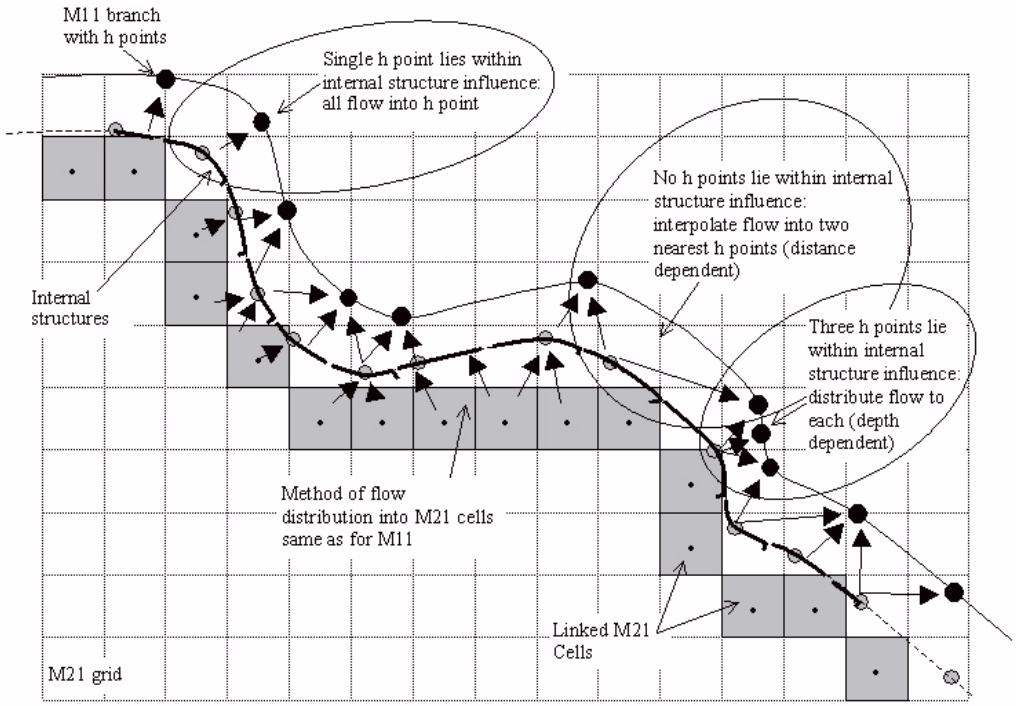

Figure 3.6: Schematization of 1D2D- flows through lateral links in MIKE FLOOD
Source: (DHI, 2014b)

3.3 Model Parameterization

The principal target of any modelling problem is the calibration of the friction coefficients. The values for bed friction were varied between 0.03 and 0.04, as are accepted for lightly vegetated channels. The channel had tall standing grasses in its bed as observed in the field. The values of flood plain friction were varied from 40 to 50 for uniform calibration. The model was calibrated for the surface roughness coefficients and the other parameter values were determined on the basis of knowledge of the model structure, field and literature. The study reach is a flood diversion channel and only has water when the causeways are breached due to flood water level rising beyond the danger mark, thus the initial global water level was given a low value of 2 m. The impact of the wind can be significant for areas with large flooding extents and long durations of flooding, e.g. several weeks or more. Since, neither was the case in the flooding events being scrutinized, the wind friction parameter was dropped from the calculations. The wave approximation was chosen as high order fully dynamic as it conserves the mass and momentum of the water spreading over the flood plain even with a very small slope. The high order fully dynamic description has specific high order and upstream centred friction terms which allow the user to specify longer simulation time steps than possible for a fully dynamic approach (DHI, 2014a). The flooding and drying depths have to be specified too, based on literature the flooding depth was chosen as 0.4 m and drying as 0.35 m as it is recommended that the difference between the two values should not exceed a few centimetres. The evaporation and precipitation terms are also important if the flooding extent and duration are of a large magnitude, they are not used either. The value of eddy viscosity was chosen as 0.8 as previous studies have shown little sensitivity to the parameter (P D Bates & De Roo, 2000) and it has been proven that artificially high values may help in stabilising the model during unsteady flow simulations (M. S. Horritt, 2000).

3.4 Data Requirements and Pre-processing

Hydrodynamic models require two types of data; inputs such as inflow hydrographs of discharge entering the channel at the upstream boundary, detailed topographic data, surface roughness values and cross- section elevation profiles; for calibration and validation such as flood extent, discharge/water level at downstream boundary.

3.4.1 River and Flood Plain Geometry

CARTOSAT - I images (Stereo pair) for 03 February 2012 were acquired for the study area. Cartosat-1, the first Indian satellite with along track stereo imaging capability, was launched in May 2005 by a PSLV-C6 vehicle. The high-resolution stereo data beamed from twin cameras onboard Cartosat-I mission facilitates topographic mapping up to 1:25,000 scale (Srivastava et al., 2007). The sensors have a spatial resolution of 2.5 m and generate in-track stereo-pairs using two Panchromatic cameras – fore (+26°) and aft (-5°) with respect to the nadir view in the along track direction (Jayachandraiah, Krishnan, Srinivas, & Kumar, 2007).

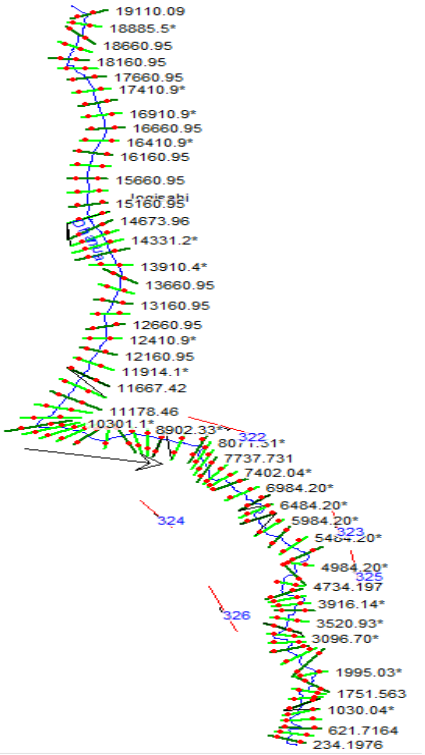

Figure 3.7: Cross sections extracted from CARTOSAT 5 m DEM

A global DEM of 30 m is offered as a ready-made product from the National Remote Sensing Centre on their 3D geo visualisation and data download website Bhuvan (National Remote Sensing Centre, Govt. of India). The metadata contains the Rational Polynomial Coefficients (RPC) for the sensor which allow for seamless triangulation at 30 m resolution and give a vertical accuracy of ± 17 m which rivals global DEMs like SRTM 3 arc-second product (± 16 m) and ASTER 1 arc-second (± 18 m). The vertical accuracy can however be improved drastically by supplementing the RPCs with Ground Control Points (GCP) acquired using a Differential Global Positioning System (DGPS), well distributed over the tile.

The ground survey for the DGPS was done using the Leica RS 500 DGPS during November, 2014. Since the average elevation of the area is very low and gently sloping, the focus was to get maximum GCPs in the area of the actual flooding, determined through a priori knowledge of the study area, gained from flood maps of the 2003 event. 24 GCPs were taken. Water marks and intrusion of silt was documented as well.

The CARTOSAT-I Stereo images of 2.5 m resolution were triangulated, ortho-rectified and a DTM was extracted using the Leica Photogrammetry Suite (LPS 2011). The Rational Polynomial Coefficients (RPC) approach was used for the triangulation using the coefficients supplied with the satellite data (Murthy, Rao, Rao, & Jayaraman, 2008). The model was fine-tuned using 2nd order polynomial adjustment (V. K. Singh, Ray, & Jeyaseelan, 2010). The 24 GCPs were identified in both the images and full (vertical + horizontal) control was assigned to them. 16 out of these were taken as control points and 8 as check points. The control points were supported by

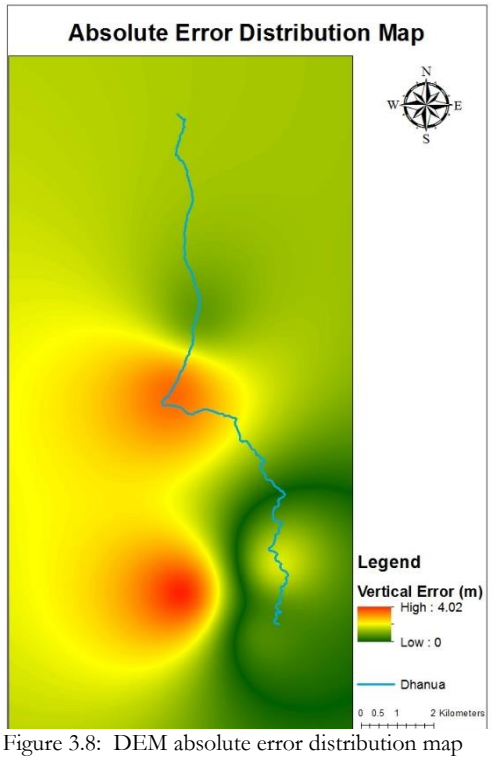

Figure 3.8: DEM absolute error distribution map

finding 200 identical tie points on both the images. The check points were used to assess the distributed accuracy of the digital elevation model. The DEM was extracted using both the classic and enhanced automatic terrain extraction techniques (ATE). The Enhanced ATE result was eventually used due to a lower RMSE value to generate the 5m DEM used to derive the river and flood plain geometry. Six of the bank elevations and bed elevations were surveyed in the field and the rest were extracted from the DEM and corrected based on interpolated cross section values.

Figure 3.7 shows the extracted cross sections for the 5m DEM. The RMSE was calculated by using some of the GCPs as check points. Since the RMSE is calculated at some isolated points it cannot be assumed to be representative for the entire grid. Furthermore the bias cannot be ascertained to be positive or negative. Due to this reason an Inverse Distance Weighting (IDW) approach having a factor of 2 was used to generate an error distribution map (Fig. 3.8), to best estimate the error for each pixel. After calculating the error the absolute value was taken as it would be representative of the actual deviation from the true elevation value. The map clearly indicates that the areas of major flooding fall in low error zones.

The main problem with the study area was that most of the area had negative values for elevation with reference to the WGS 84 global ellipsoid. Both the DGPS and the Stereo images were using the WGS 84 ellipsoid as reference and thus, giving negative values. As we know the global ellipsoid finds the best approximation of the earth's geoidal surface, as shown in fig. 3.9. Owing to this, some regions have negative elevation values, especially in the coastal regions. The ellipsoid over the Indian coastline shows a positive deviation of 60 – 63 m from the mean sea level (m.s.l.) thereby showing all elevation values ≤ 60 m as negative. This causes problems in the pre-processing stage during stream definition and catchment delineation. To rectify this, the EGM (Earth Gravity Model) 96 (Lemoine et al., 1998) geoidal surface was used, which gives elevation values with reference to the global mean sea level. The EGM 96 correction was done in ArcGIS where the distributed ellipsoidal deviations in grid form were subtracted from the DEM to get positive values in the study domain.

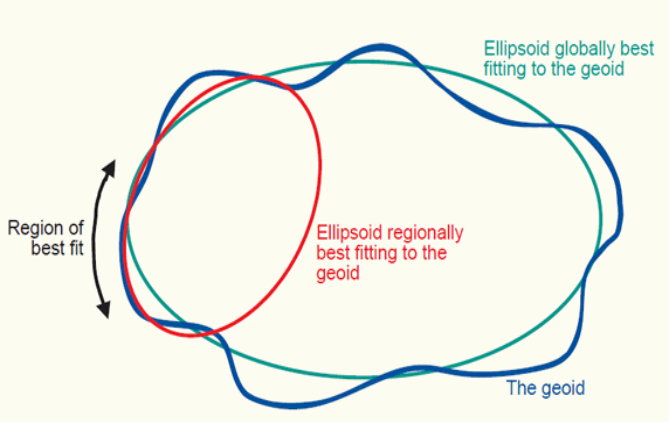

Figure 3.9: Ellipsoidal approximation of Earth's geoidal surface
Source: http://kartoweb.itc.nl/geometrics/reference%20surfaces/body.htm

Finally, the 5 m DEM was used to extract cross sectional topography. MIKE FLOOD uses the DEM grid resolution as the spatial unit for the solution domain. As discussed earlier, while it has been proven that a high resolution model bathymetry with detailed topographical information can give better results, the cost in terms of simulation time increases exponentially. MIKE FLOOD also has a limitation that the Courant Number should not exceed 0.5, as it renders the model unstable.

$$C_R = \frac{(v+\sqrt{gd})\Delta t}{\Delta x} \quad \text{.....Equation 3-6}$$

Where, v=velocity; g=acceleration due to gravity; d=water depth; Δt=time step and Δx=grid spacing. The Courant number condition defines a delicate relationship between the time step and grid size. On the basis of literature and the available time, the combination of a 15 m grid size and a 2 second time step was taken as the optimum.

In order to generate a DEM of 15m resolution it had to be resampled from its original resolution of 5m, which essentially meant that a resampling technique had to be chosen. In order to do that objectively, the resampling techniques were first compared with each other. 250 points were distributed randomly over the DEM and the elevation value was extracted for all the different resolutions using different resampling

methods. The original DEM values were assumed to be true and the root mean square error, mean absolute error and the maximum error were calculated for the deviations in the resampled DEMs. The effect of DEM resolution on the model was not studied as there have been numerous studies that have proved that hydrodynamic model performance improves with increasing DEM resolution (Alemseged Tamiru Haile & Rientjes, 2005; Sanders, 2007).

S. No	Parameter	Specification
1	Nominal Altitude (km)	618
2	Swath (km)	30 Fore, 27 Aft
3	Local time for equatorial crossing	10:30 AM
4	Instantaneous Geometric Field of View(IGFOV) (m)	2.5 x 2.7 Fore 2.22 x 2.23 Aft
5	Spectral Bands a) No. Of bands b) Bandwidth (μm)	 1 Panchromatic 0.5 – 0.85
6	Quantisation in no. of bits/pixel	10
7	No. of detectors	12000 per camera
8	Compression	JPEG Like, 3.2:1
9	B/H Ratio	0.62

Figure 3.10: Sensor characteristics of CARTOSAT-I (Srivastava et al., 2007)

3.4.2 Characterization of Bed and Floodplain Friction

Bed and flood plain friction or resistance, oppose the flow of water. These values usually depend on the type of land use or vegetation type, based on which surface roughness and the impedance to flood flow can vary (Werner et al., 2005). There are several different coefficients for surface roughness such as Manning's n, Manning's M, Chezy numbers, etc. each of which are equally acceptable for the accurate representation of the surface roughness. Chezy's numbers are related to the Manning's values by the following relationship:

$$C = \frac{R^{\frac{1}{6}}}{n} = MR^{\frac{1}{6}} \quad \text{.....Equation 3-7}$$

Where R is the resistance (or hydraulic) radius and C, M and n represent Chezy's and Manning's numbers respectively. The difference between the Chezy's and Manning's description is the power of R. As apparent from the above equation M and n are independent of depth whereas the value of C varies with depth (DHI, 2014c).

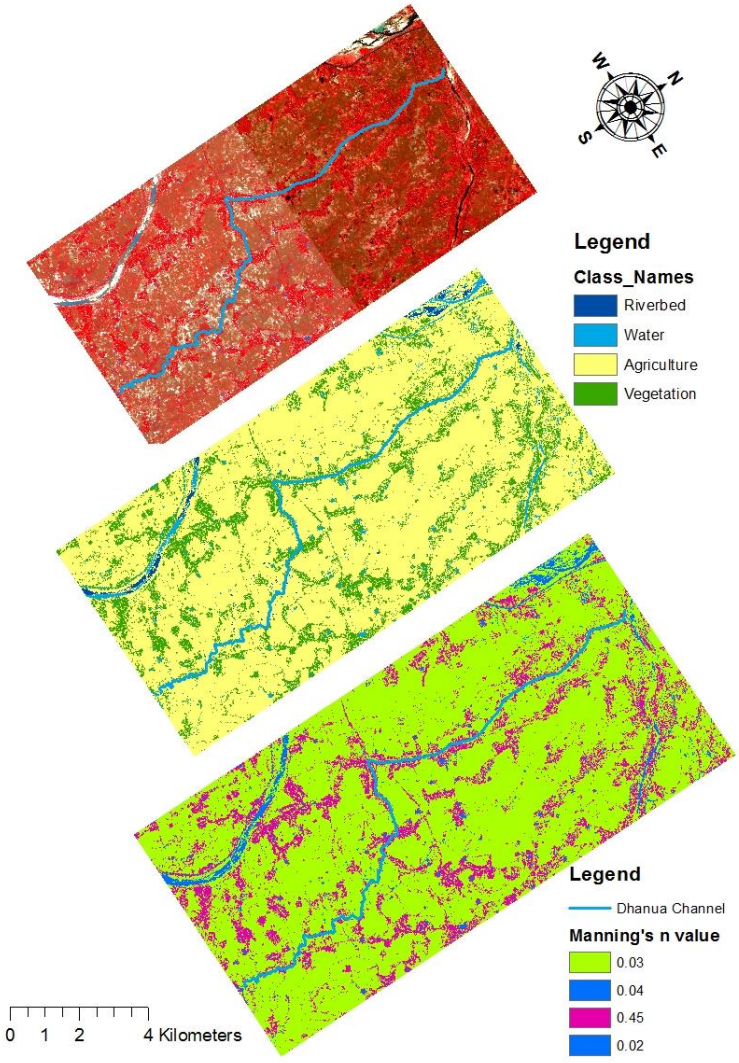

Figure 3.11: Roughness Distribution Map

In this study the widely used Strickler Manning's Roughness Coefficient, has been calibrated. Values have been listed in literature dating back decades, based on channel and floodplain characteristics which can be inferred from remotely sensed data. The values of n is characteristically in the range 0.01 for a smooth channel to 0.1 for a thickly vegetated channel and Manning's M for the floodplain between 10 to 100 (DHI, 2014c). A distributed roughness map can be prepared for the flood plain as a model input, assigning separate values to each land use based on literature (figure 3.11). The land use map was generated using high resolution multispectral data LISS-IV (5.8 m). The accuracy assessment was done using a random sampling of 500 points. As the majority of the area is agricultural land, systematic random sampling would have assigned an equal number of points for assessment in each class, whereas agriculture needs to be prioritized. The kappa statistic for the classification was found to be 0.92. The over 90% of the study area consists of cultivated land apart from water bodies and rural settlements surrounded by heavily vegetated patches. The information gathered during the field visit indicated a cropping cycle according to which the fields are kept empty during peak monsoons due to flood risk and to avoid flood damage. Barren fields have a different range of values for 'n' (0.02-0.03), which was also considered for the calibration.

3.4.3 Boundary Conditions

The boundary conditions define the interaction between the external environment and the modelled system. Hydrodynamic models ordinarily require constraints at the upstream and downstream locations of the study reach. In this study the discharge hydrographs were provided for 2003 and 2014 as shown in figure 3.12 and 3.13 respectively. Lateral inflow data can also be provided to the model as a boundary, if available. Scientifically, boundary conditions can be of three types: Dirichlet condition (specified head boundary), Neumann condition (specified flow boundary) and Cauchy condition (head-dependant flow boundary) (Alemseged Tamiru Haile & Rientjes, 2005).

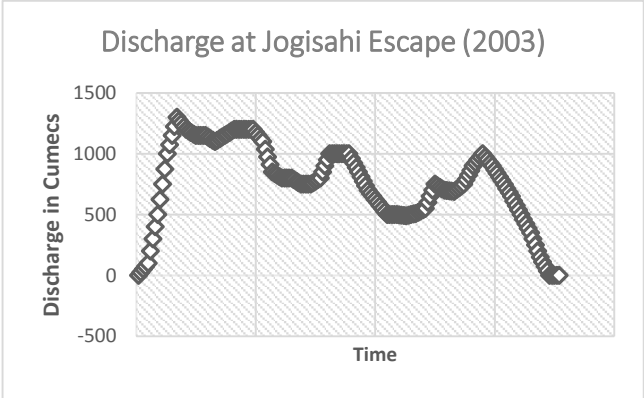

Figure 3.13: Upstream boundary condition, 2003 hydrograph (Calibration) Source: Orissa WRD

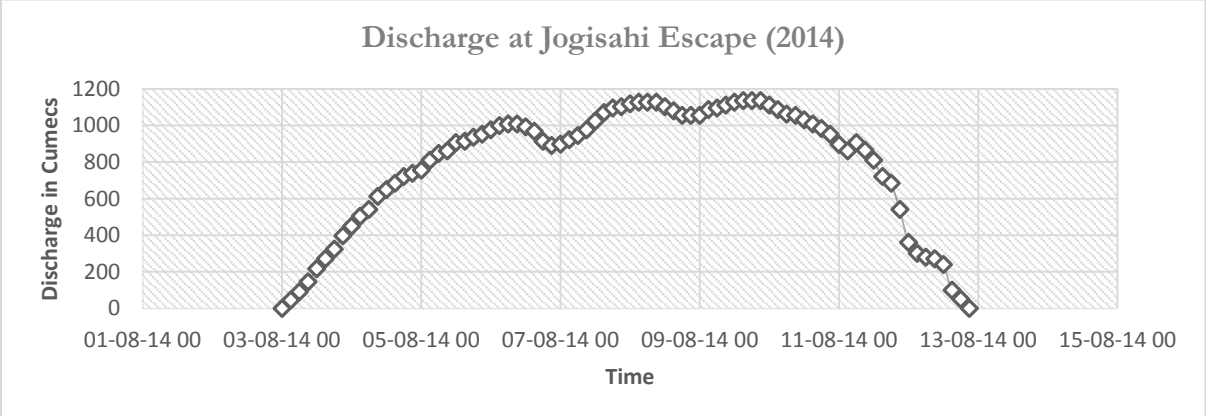

Figure 3.12: Discharge Hydrograph at Jogisahi Escape (Validation) for 2014

The available boundary conditions in MIKE FLOOD include flux, water level and rating curves. At the upstream boundary the Neumann condition was used, i.e. the flow over the duration of the simulation period was provided as an inflow hydrograph. The upstream boundary does not have a gauge at its exact location. The data was obtained at the Mundali gauging station at 20°26'44.87"N and 85°44'42.87"E located 30 m above m.s.l. The data that served as the boundary condition was flow that was observed during the

29th of August 2003 to 6th September, 2003 when the peak flows were observed, readings of flow at 3-hourly intervals were provided. For the purpose of validation discharge data for the 31st July, 2014 to 11th August, 2014 at 3-hourly interval was used. This is the specified flow boundary, often referred to as the Neumann condition. Using this, the flow at the causeway was calculated, by the side weir formula and the water distribution percentages given by the Water Resource Department, State Government of Odisha (WRD).The intial conditions of the channel defines the behaviour of the channel to a large extent. As we proceed further into the simulation time the influence of the initial conditions diminishes rapidly until the channel flow is completely independent of them. The effect of these was not studied as many studies have time and again proven the above fact (Alemseged Tamiru Haile, 2005). For the downstream boundary condition hydraulic free flow condition was specified by assigning a constant water level at the boundary lower than the bed level. This is the Dirilecht condition, specified head boundary. One tenth of the total simulation period was, used as the warm up period for model stabilisation.

3.4.4 Flood Boundary Delineation

Several methods of flood identification using remote sensing data have been prevalent since the advent of aerial photographs. The chief ones have been discussed by Paul D. Bates, in his review article in 2012. These can primarily be classified into four kinds of techniques, visual interpretation, image thresholding techniques, image texture algorithms and multi-temporal change analysis (Guy Schumann, Bates, et al., 2009).

3.4.4.1 SAR Data Processing

RISAT-I Medium Resolution ScanSAR (MRS) for 9th August, 2014 and RADARSAT – II ScanSAR narrow of 4th September, 2003, were the datasets used for the identification of the inundation extent. RISAT (RADAR Imaging Satellite) 2 uses the X band for data acquisition as opposed to the C band used in RADARSAT II. The respective spatial resolution of the RISAT I-MRS and RADARSAT-II SAR datasets were 18 m and 50 m. The HH and HV products were both acquired but HV was used due to its established value for inland flooding applications and lesser visible speckle effect (Al-Ali, 2011).

The imported Single Look Complex (SLC) datasets were multi-looked with an azimuth looks 1 and range looks 1. The geo-referencing and terrain correction were done using the DEM generated from CARTOSAT data for this study, as it had the highest vertical accuracy. SAR data usually has rectangular pixels and thus needs to be resampled to square grid for further processing. SAR images have to be filtered to remove the speckle noise. In order to remove the salt and pepper effect, Equivalent Number of Looks (ENL) has to be estimated. A sample of pixels having a low variance is chosen from the flooded part of the image thus the main contribution is from speckle.

$$ENL = \frac{1}{(Coff.\ of\ variation)^2} \quad \text{.....Equation 3-8}$$

The geo-referenced images were filtered using a 5X5 Frost filter (Matgen, Schumann, Henry, Hoffmann, & Pfister, 2007). The filtered images are converted to backscatter file in Decibels (db.) units by using the following formula

$$Db = 10 * alog(float(b)); \quad \text{.....Equation 3-9}$$

Where b is the geo-referenced filtered image.

3.4.4.2 Generation of Flood Maps

The last few years have witnessed a steady rise in the number of flood studies which used SAR derived flood boundaries for calibration. The advent of these spatial calibration techniques helped to do away with the dilemma of validating 2 dimensional data with point hydrometric data (Baldassarre & Schumann, 2011). As the need for SAR based flood maps increased, many techniques were proposed based on the

aforementioned broad themes. However, due to the unavoidable subjectivity in each of the approaches, it cannot be claimed that one might perform better than another (Guy Schumann, Di Baldassarre, et al., 2009). Most methods are able to distinguish flooded pixels in the centre of the flooded area, the ambiguity creeps in when a boundary has to be delineated. Due to the differences in the tone and texture at the edges of the flood, where the depth is low and some backscatter may be due to the underlying vegetation, etc. it becomes impossible to demarcate a boundary with any certainty (Di Baldassarre et al., 2009). In this study, an approach which accounts for this uncertainty was used.

Four maps were created using visual interpretation, radiometric thresholding and texture based co-occurrence filters (variance and homogeneity) for each event. All the maps were edited afterwards by comparing with optical data from Google Earth and MODIS, for the edges and problematic areas e.g. near vegetation patches. Each of these maps were assigned equal weights and a possibility of inundation (POI) map was created (M.S. Horritt, 2006). Each pixel of the POI map had a value representing the possibility of flooding for that event. If the pixel was flooded in only one of the maps then it would have a $P_{i,j}$ of 0.25 and if it was flooded in all four, the $P_{i,j}$ would be equal to 1 (Mason et al., 2009).

3.4.5 Calibration Techniques

Each simulation run for model calibration was carried out using a time step of 2 sec and a model domain resolution of 15 m which was found to be the best in terms of simulation time and model performance. Every simulation took approximately 14 hours for a normal run completion. The satellite overpass time for RADARSAT II for the study area was 10:30 AM on the 4th of September 2003. MIKE Zero offers the functionality of exporting the static map for a particular time step in the simulation period as an ASCII file, which can then be imported in a tiff format. ENVI read ASCII function was used to add the projection information to the said ASCII file and save it in a raster format. The output is in the form of floating point values of water depth in metres, which was then reclassified into a binary map, flooded/non-flooded for further comparison and analysis.

Numerous novel calibration techniques have been proposed over the years for the use of binary flood maps for model calibration. In this the following approach, proposed by M.S. Horritt, 2006, was used. The POI map was classified into regions of similar probabilities and the proportion of simulated wet cells in each region were counted. In a perfect model, the proportion of simulated wet cells in each region would match the value of possibility, e.g. 50% of the cells having a possibility of 0.5 should be simulated as flooded. These were plotted as reliability diagrams (simulated proportion vs. possibility of inundation) where the 1:1 line would be given by an accurate model (Di Baldassarre et al., 2009). The accuracy can be assessed using the deviation of the actual line from the 1:1 line, weighted by the number of cells in that class (M.S. Horritt, 2006).

Many objective functions have been created to assess model performance spatially. The table used for these is given below:

Table 3.1: Contingency table

	Present in observation	**Absent in observation**
Present in model	A	B
Absent in model	C	D

The objective functions currently in use, summarized by Guy Schumann, Bates, et al., 2009, have been presented in Table 3.2. Most of these have been used widely for assessing model performance spatially. F(2) is the one most abundantly used in deterministic calibration studies (Di Baldassarre et al., 2009; M. S. Horritt, 2000; M.S. Horritt, 2006). However, for this research Bias and F(1) have been used as they have been recommended for uncertain calibration (Guy Schumann, Bates, et al., 2009).

Table 3.2: Objective functions used in model calibration (modified from P D Bates & De Roo, 2000)

S. No.	**Objective Function**	**Equations**	**Recommendations**

1	Bias	$\frac{A+B}{A+C}$	For aggregate model performance (optimum value 0)
2	Receiver Operating Characteristics (ROC) Analysis	$F = \frac{A}{A+C}$; $H = \frac{B}{B+D}$	Summarizes under-prediction and over-prediction and is potentially a useful tool for exploring their relative consequences and weighting in any subsequent risk analyses.
3	F(1)	$\frac{A}{A+B+C}$	Recommended for both deterministic and uncertain calibration. A relatively unbiased measure that equitably discriminates between under-prediction and over-prediction. As such, optimal simulations will provide the best compromise between these two undesirable attributes. (Optimal value = 1)
4	F(2)	$\frac{A-B}{A+B+C}$	Recommended for deterministic calibration (if under-prediction is preferable). Explicitly penalizes over-prediction but suffers as a result during uncertain calibration. Over-predicting simulations are wrongly retained to offset the bias introduced by the measure and provide an acceptable compromise between inundation map accuracy and precision. The benefits of rejection are reduced accordingly. (Optimum value = F(1) and close to 1)
5	F(3)	$\frac{A-C}{A+B+C}$	Recommended for deterministic calibration (if over-prediction is preferable). It is not sensitive to domain size and appears to favour over-prediction similar to PSS. (Optimum value = F(1) and close to 1)

4. RESULTS AND DISCUSSION

4.1 SAR Based Flood Maps

As elaborated in section 3.4.4.2 of this thesis, many different approaches were used in this study to extract the flood extent from the SAR images, chiefly to encompass the apparent subjectivity. The texture based classification was however found to have the maximum agreement with the model simulations in this study, having significantly higher measure of fit values than the other two techniques for the calibration.

4.1.1 Visual Interpretation

The first method used was visual interpretation, which did not give the best results. The reason for this was that the SAR image was of a time after the peak flood, during the time of the recession of the flooding. Due to this reason the number of isolated flooded pixels were quite high which could not be identified and demarcated visually. Another important factor to consider is that in remote sensing data any pixel having even a thin undisturbed film of water over it is also detected as a flooded pixel because of specular reflection off of the smooth surface. Conversely, microwaves have a different interaction which urban and highly vegetated land uses which elicits different responses like volume and double bounce (corner) scattering which makes it hard for them to detect water pixels near such areas. Previous studies advise to remove these areas of uncertainty from our calibration domain by assuming them to be NoData pixels (Hostache et al., 2009). However, as the non-flooded pixels have not been considered as contributing to any of the goodness of fit measures, in this study they have been included with the non-flooded pixels. It is equally important for a model to correctly predict the dry areas as dry, as it is for the model to correctly identify the wet areas as wet, nonetheless, the dry regions have not been considered for this study. The primary reason for this was that the order (magnitude) of the dry pixels is much higher than the wet ones and it is relatively easier for models to predict the dry areas, thus measures of fit including this parameter gives a falsely optimistic view of the model performance (P D Bates & De Roo, 2000).

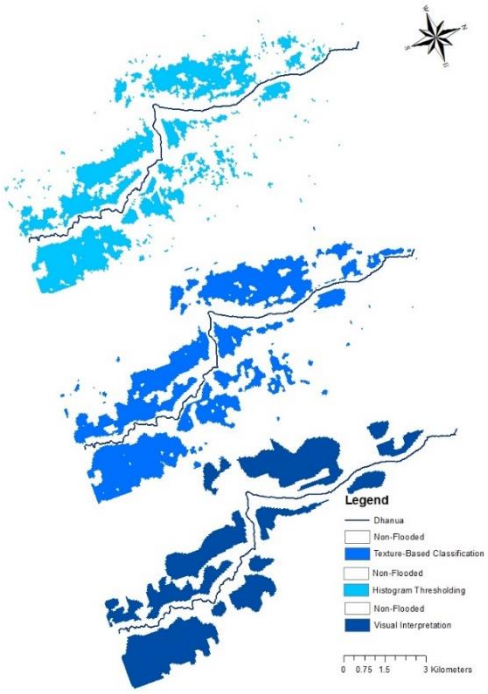

Figure 4.1: The different flood maps derived from the RADARSAT-II Data for 4th September, 2003

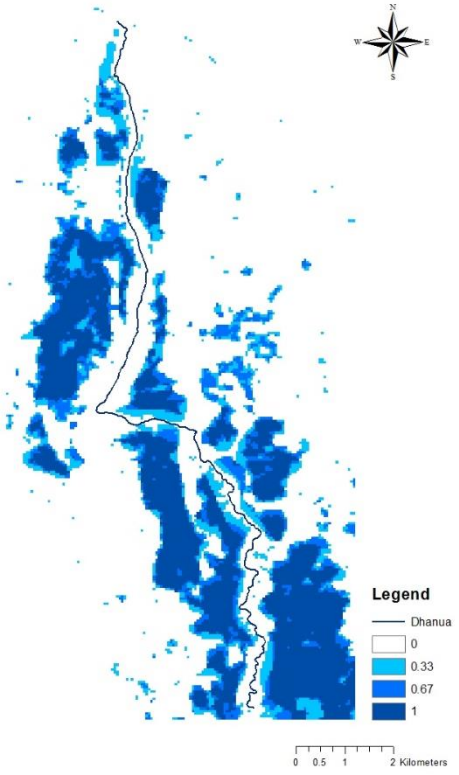

Figure 4.2: Possibility of Inundation Map for 4th September, 2003

4.1.2 Texture Based Classification

For the texture based classification two filters were used namely the variance and the homogeneity filters, which were found the most suitable. The flooded areas have comparatively more homogenous image statistics than the non-flooded areas having varied land- use types, it is due to this reason that the aforementioned filters were chosen. Using this property of the image the flooded areas can be extracted. The texture based map could easily differentiate between the flooded and non-flooded pixels even in areas where the thresholding gave ambiguous results. This is mainly because the texture based maps don't pick out non-uniform areas like isolated wet pixels outside of the main area of flooding which may be cause due to other factors such as rainfall or any reasons other than channel flooding.

4.1.3 Histogram Thresholding

Histogram or radiometric thresholding is the most primitive and the simplest approach to flood delineation from remote sensing data. Image histograms for flooded areas are usually bimodal. The value at the trough of this bimodal histogram was chosen to classify the image into a binary flood map. The problem with such an approach is that some speckle errors in SAR data that the filtering couldn't remove are misclassified as flooded pixels. These equivocal pixels need to be reclassified manually to the non-flooded category, by recoding. For the 2003 event a DN image was used and the threshold was set at 48 after testing various other thresholds for suitability. The 2014 image was used in the backscatter format i.e. db values and the threshold value was fixed at -9.8 db after testing various other values.

4.1.4 Possibility of Inundation Maps

The possibility map was derived by adding all the three binary flood maps and diving the output by three. This process gave us the possibility value ranging from 0 to 1 for each pixel, based on how many of the maps had classified it as flooded. This information was found to be very useful in assessing model performance. The technique allows us to validate the model using the uncertain observations of flood extent while accounting for the uncertainty simultaneously. The figures 4.1, 4.2, 4.3 and 4.4 depict the various flood maps thus generated and the possibility of inundation maps as well, for the 2003 and 2014 flood events respectively.

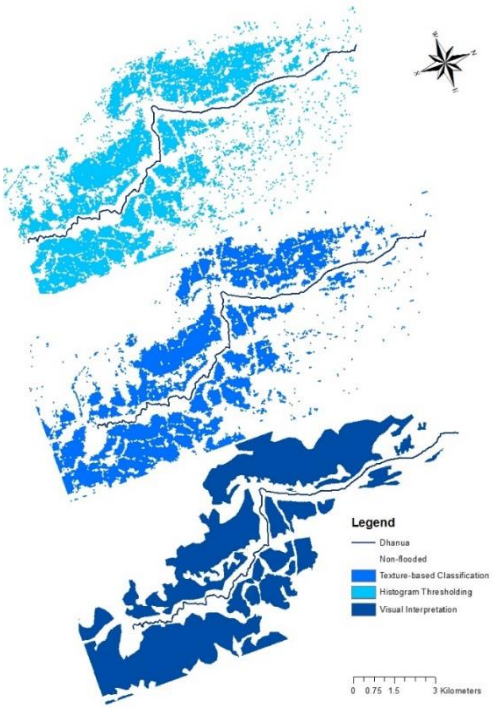

Figure 4.3: The different flood maps derived from the RISAT-I Data for 9th August, 2014

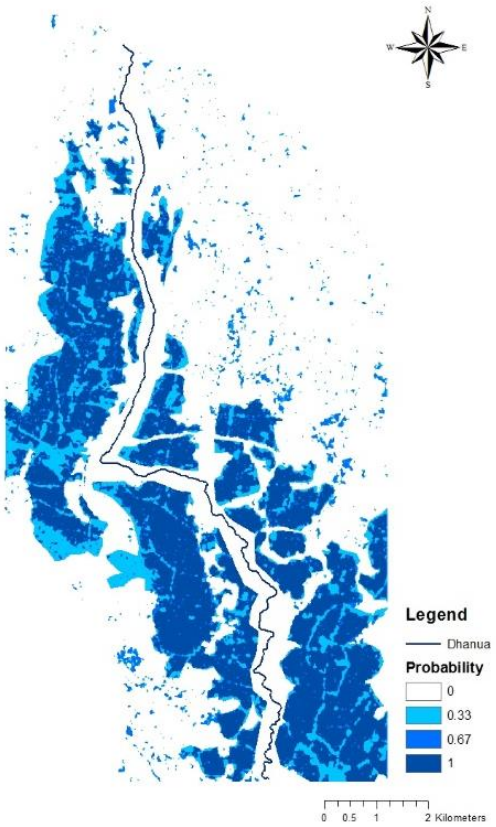

Figure 4.4: Possibility of Inundation map for 9th August, 2014

4.2 DEM Optimization for a Hydrodynamic Model

4.2.1 Comparison of DEM Resampling Techniques

The goal of the DEM construction processes is to best represent topographic parameters such as the slope of the flood plain. Resampling the DEM to a coarser grid, means the disparity in the cell sizes doesn't allow a one to one association between input and output pixel values (Alemsged, 2005). This essentially means that no single input pixel value is sufficient to represent an output grid element and therefore two or more input cells are used to estimate it. This approximation can be done using one of three resampling techniques; the nearest neighbour approach in which the output grid cell is assigned value of the input pixel whose cell centre is the least distance away from the output cell's centre; bilinear interpolation in which the nearest 4 cells are averaged to get the output pixel value; and cubic convolution in which the nearest 16 pixels are averaged. While the nearest neighbour approach preserves original values, some of the input pixel values may have no representation whatsoever in the output, the bilinear approach, makes the DEM smoother due to the averaging and the cubic technique results in both sharpening and smoothening of the image in different areas.

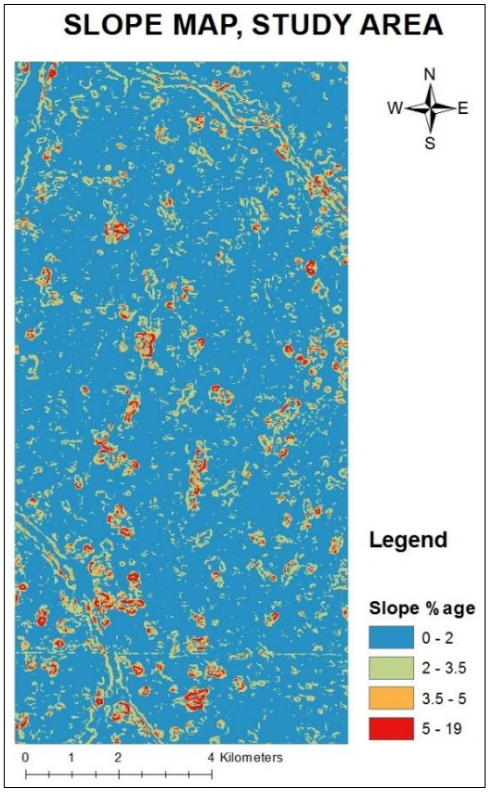

Figure 4.5: Slope map of the study area

It has been demonstrated that the choice of resampling techniques can have a significant impact on the results as the slope can vary greatly with resolution. Alemseged Tamiru Haile, 2005, found that in smaller grid sizes such as 4.5 – 7.5 m, the averaging by bilinear and cubic methods was causing substantial losses in information and introducing a notable amount of error. Wu et al., 2008, studied the effects of the errors introduced in topographic parameters due to DEM interpolation techniques comprehensively. They too found that the averaging applied by both bilinear and cubic procedures can introduce synthetic irregular surfaces at the edges of features and higher slope values overall. Alemseged Tamiru Haile & Rientjes, 2005, illustrated that while degrading the grid size of the DEM introduces some inherent error in the DEM values, the choice of the resampling method did not have much impact on the results.

In the chosen study area though, the gradient of elevation is so low that the averaging doesn't seem to have as profound an impact as found in previous studies. Figure 4.1 depicts the slope percentages in the study area. It is clear from the image that the average slope of the area is less than 2%. It is only near some of the levees and roads that the slope is higher.

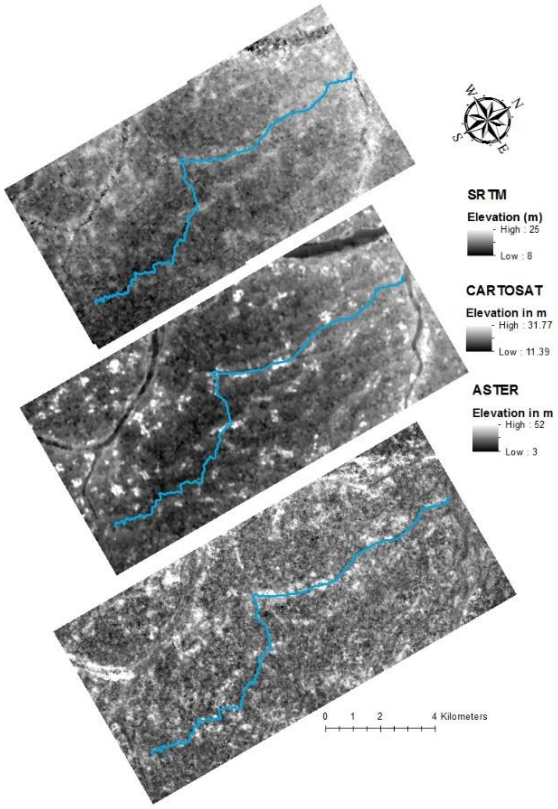

Figure 4.6: From top to bottom the SRTM (90m), CARTOSAT (15m) and ASTER (30m) DEMs

The change in slope due to resampling can mainly be attributed to the fact that the distance between cell centres in a larger grid size increases and there is an abrupt change in the values of adjacent pixels instead of a smooth transition with minor changes in the values as can be expected in smaller pixel sizes. Table 4.1 summarizes the findings of the comparison between different resampling methods. The RMSE shows a common trend of increasing with increasing grid size for all the tested approaches. For the 15 m resolution, cubic showed the minimum amount of error, however no significant impacts of the resampling method chosen were visible. The findings are not in keeping with previous findings, as the topography of the study area is very flat, with minimal slope and no sharp elevation changes. The average elevation of the area is very low and nearly similar which is why the resampling techniques are not showing a great effect on the RMSE. The range of values for the bathymetry file used for MIKE FLOOD was from 12.5 to 30 m.

4.2.2 Optimization for Flood Modelling

The final DEM had a vertical root mean square error (RMSE) of ± 2.53 m and the horizontal accuracy of 0.175 pixels (± 0.625 m). For the channel bathymetry, the bed elevations for the channel were interpolated using the Inverse Distance Weighting approach, using a factor of 4 instead of 2 as it was found to be the optimum for channels with gentle slopes in a study conducted by Tarekegn in 2009. He proved unequivocally using derived slope percentages and the RMSE values that the factor of 4 outperformed the commonly used factor of 2. The channel geometry is one of the most important contributing factors in determining the flow vectors and more often than not it is not accurately captured by the remotely sensed elevation models. The ground surveyed cross section information is needed to aid the DEM to generate correct flow path, especially in areas having a low elevation gradient as the direction of flow derived from the contours can be rather ambiguous. In case of the present study, the significance of burning it in the DEM is reduced as we have used a 1D approach to model the channel but it is required for the cross section information in 1D and helps to regulate the flow over the lateral linkages connecting the 1D and 2D model domains.

Table 4.1: Results from comparison of resampling methods

Method	Grid Size (m)	Maximum Error (m)	Standard Deviation (m)	RMSE (m)	MAE (m)
Nearest Neighbour	10	0.654	0.164	1.183	0.090
	15	0.673	0.154	1.090	0.096
	20	1.493	0.300	2.174	0.148
	30	1.154	0.263	1.871	0.162
Bilinear Interpolation	10	0.321	0.088	0.628	0.062
	15	0.673	0.154	1.090	0.096
	20	0.999	0.224	1.623	0.138
	30	1.070	0.259	1.865	0.166
Cubic Convolution	10	0.338	0.085	0.609	0.059
	15	0.670	0.152	1.081	0.097
	20	1.032	0.226	1.635	0.137
	30	1.100	0.263	1.896	0.166

4.3 Model Sensitivity Analysis

4.3.1 Sensitivity to Downstream Boundary Condition

The effect of both downstream boundary conditions and the initial conditions is minimised as we move further away from the point at which the condition is applied. The effect of the boundary condition was investigated on only the 1D model component due to simulation time requirements. Figure 4.7 shows the maximum water surface profiles for various types of boundary conditions available in MIKE 11. The analysis revealed that the boundary conditions showed a significant effect only near the downstream end of the channel. As the study reach is short in length the boundary effects almost half of the area of interest. For the actual channel slope, the maximum water depth became independent of the downstream boundary condition at a distance of 7.328 km after the point at which the boundary was specified. When the bed level is artificially made steeper to test the influence of cross section density on the conveyance in the channel it is seen that for a greater slope and sparsely distributed cross sections the channel geometry is not accurately captured. One of the simulations was also done by taking a rating curve at the outlet, auto-generated by MIKE. This test also shows no deviation from the free flow condition specified at the downstream boundary. The hydraulic free fall condition is specified in MIKE 11 by specifying a water level lower than the elevation of the last cross section at the boundary. The effect of the boundary condition is also determined by the surface friction values for the channel and the flood plain.

From this test it can be seen that the MIKE 11 1D model is extremely sensitive to the boundary conditions at the specified location but the sensitivity decreases as we move further away from it. Thus, in case of bad data at the boundary it may be prudent to apply the boundary condition several kilometre downstream of the actual reach of interest, thereby minimising the effect of the same.

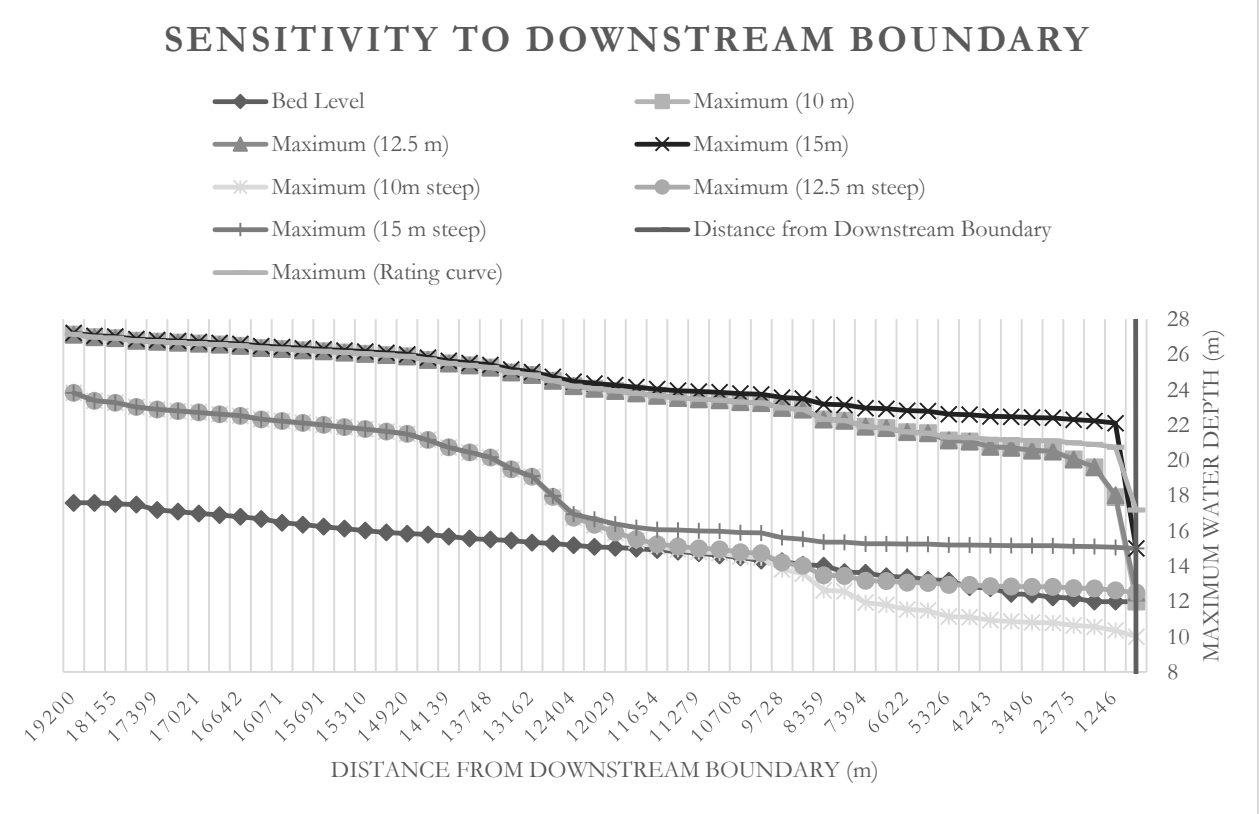

Figure 4.7: Maximum Water Level profiles for different types of boundary conditions using unsteady flow simulation

4.3.2 Sensitivity to the Surface Roughness Coefficients

The surface roughness coefficient, most commonly the Strickler Manning's is essentially the calibrating parameter of a hydrodynamic model. The MIKE model was found to be very sensitive to both the channel and the flood plain friction. The model is capable of taking distributed frictional values as well as constants, in either Manning's M (reciprocal of Manning's n) or Chezy's numbers. The values were varied from 10 – 90 (Manning's M) (DHI, 2014b) and a distributed roughness map was used as well but the results did not improve significantly over uniform parameterization. This might be because most of the flooded area is agricultural land and not much variation in real friction values is present on the flood plain. M. S. Horritt, in 2000 illustrated that distributed floodplain friction enhanced model performance by a mere 0.3%. The postulation of uniform frictions over channel and floodplain makes the calibration problem more practicable.

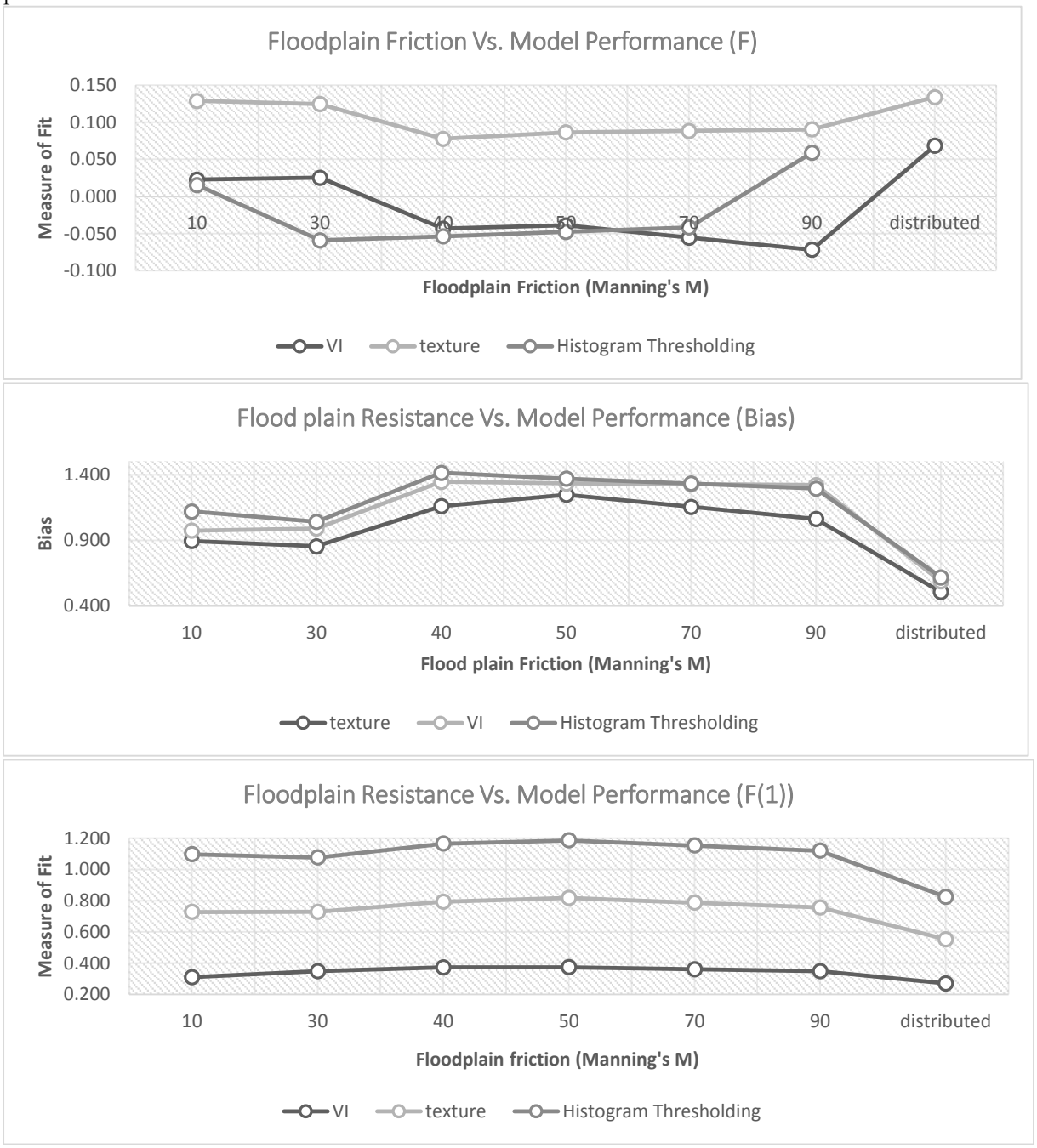

Figure 4.8: Graphs depicting the model's sensitivity to floodplain roughness values in Manning's M

Figure 4.8 shows the relationship between model performance indicators and variation in floodplain surface roughness values. It is evident from the graphs that distributed friction values are not helping the model's predictive capabilities significantly. However, it showed a significant reduction in over-prediction which is why the value of F were higher but the correctly identified wet pixel ratio did not increase. The surface friction reduces with increasing manning's M numbers as it is the reciprocal of n. Since, in reality the study area comprises of cultivated lands that are fallow in the monsoons, the floodplain offers very little resistance to the flow of flood water over it. The maximum no. of wet pixels are correctly classified around an M value of 40 beyond which the model performance becomes nearly independent of this value. The reason for this is that the maximum spread possible with the specified amount of water in the upstream hydrograph is already achieved at 40, beyond that no matter how much the roughness is reduced the inundation extent will not change significantly.

Table 4.2: RMSE value derived from reliability diagrams for the sensitivity analysis of channel and floodplain roughness

FP friction - Manning's M ($m^{1/3}/s$)	RMSE	Bed friction - Manning's n ($s/m^{1/3}$)	RMSE
10	0.755	0.02	0.390
30	0.492	0.04	0.390
50	0.340	0.06	0.266
70	0.361	0.08	0.254
90	0.383	0.1	0.254
Distributed	0.755		

The RMSE values were calculated using the deviation of the actual values from the expected 1:1 line in the reliability diagram based on the observed and predicted possibility of flooding of a particular pixel. For bed friction the minimum RMSE value was observed at 0.08 but these values were not used for calibration as they exceeded the acceptable range of values for a lightly vegetated channel. The minimum RMSE for flood plain friction was at M=50 which was used for calibration as the accepted value for barren land is around the same.

Figures 4.9 and 4.10 shows the effect of channel friction on various measures of fit enumerated earlier, objective function F(1), relative bias and F. Simulations were carried out for bed friction values varying from 0.02 to 0.1. The accepted Manning's n values for a lightly vegetated channel are within the interval of 0.03 to 0.04 (DHI, 2014a). The graphs also show a better agreement in the maps generated based on texture. This is because the texture based maps were able to best represent the maximum inundation extent, which is why the 1:1 match in texture classification was found to be better. In visual interpretation, the standalone flooded pixels cannot be delineated separately and in histogram thresholding, a higher threshold was including areas that were clearly dry, as observed in the processed SAR image.

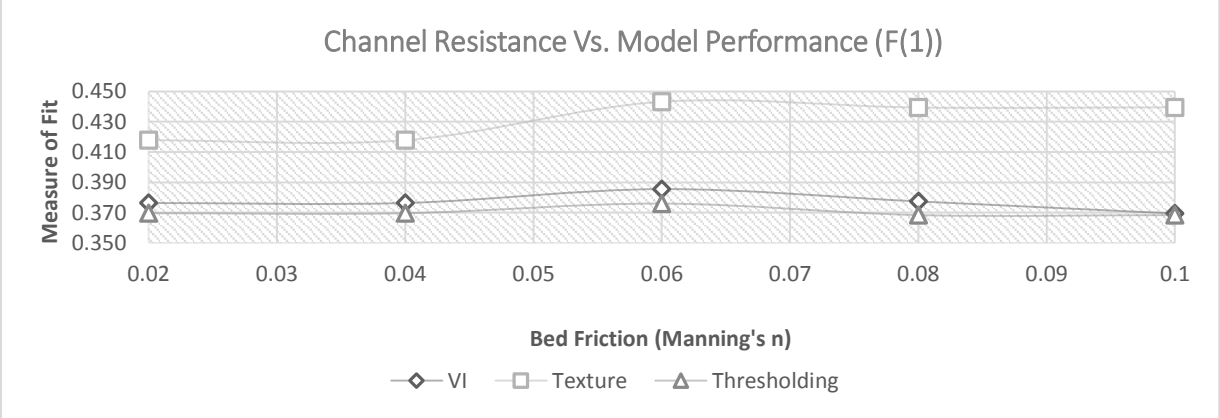

Figure 4.9: Graphs showing model sensitivity to the channel friction values

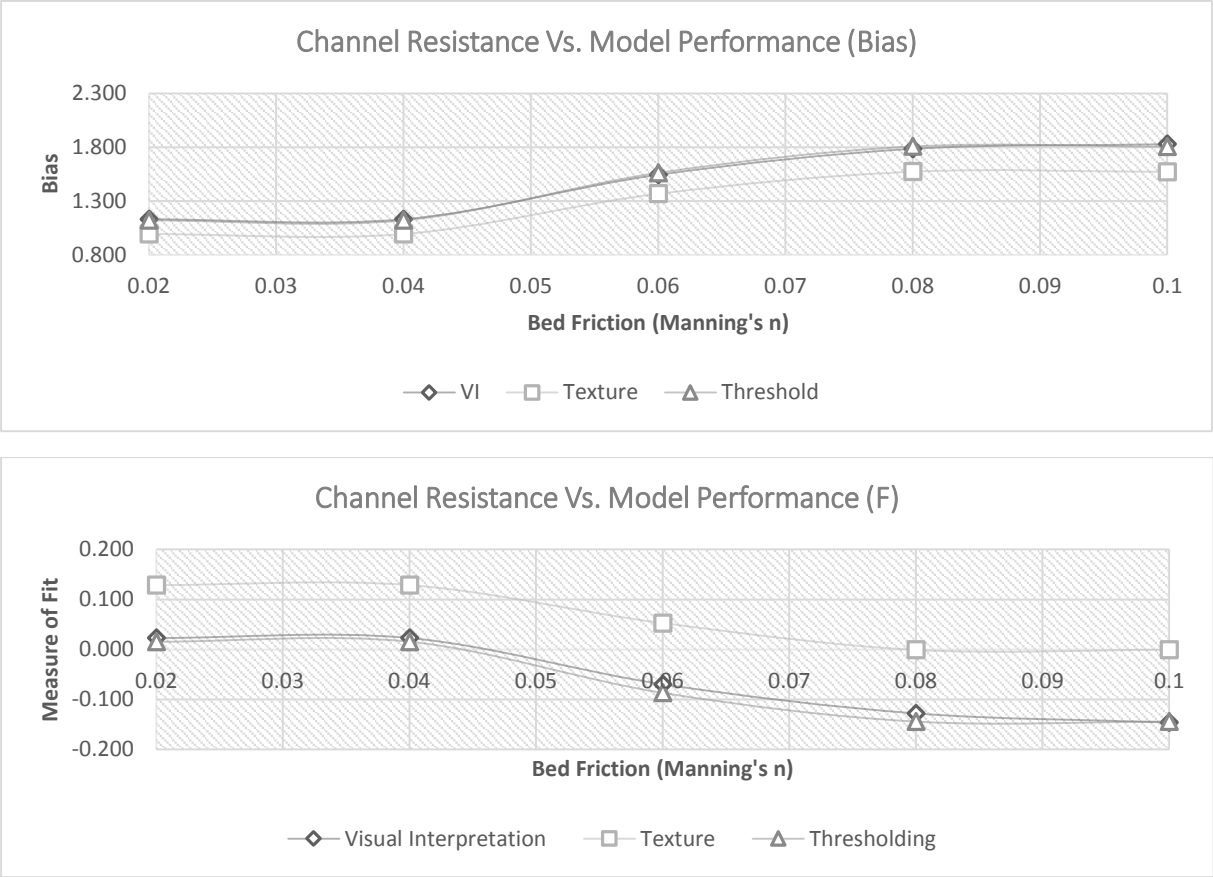

Figure 4.10: Graphs showing model sensitivity to the channel friction values

The choice of one optimum parameter set is impossible as several possible combinations may perform equally well. To deal with inherent model uncertainties in the process representation, parameterization and validation is a complex task. One of the simplest approaches were used here where it is assumed that a single optimal value for the surface roughness coefficient exists which minimizes the disagreement between the simulated and observed flooding extent (M. S. Horritt, 2000). However, given the uncertainties present in the data, a large ensemble of simulations each varying the calibrating parameter by a minute value may be more fitting. Each of the parameters can then be represented with a likelihood figure based on the values of the chosen objective functions. The Generalized Likelihood Uncertainty Estimation procedure, GLUE (Beven, 1993), which uses Monte Carlo simulations to assess the effects of uncertainty in the hydrodynamic models, is based on the same approach. While this is the best way to approach the flood simulation problems, knowing that the input data and the models themselves are ridden with uncertainties, the cost in terms of simulation time, increases drastically. Automated tools for running multiple simulations simultaneously exist more for 1D- models than 2D or coupled ones. So far not many proprietary flood models have provided tools to calibrate the model using spatial information or objective functions based on the spatial agreement between the observed and predicted extent of inundation.

A comparatively more straightforward, standard deviation method was chosen for this study, mostly due to time constraints which relies on a small ensemble of simulations. The parametric uncertainty band has been defined by a value of one standard deviation above and below the mean of the parameter values used in the ensemble. While this is a relatively simplistic approach it allows a rapid sensitivity assessment of the model to important parameters and speeds up the calibration process. This was a major advantage as limited time was available for the research. Remote sensing data has increased the dimensionality of the parameter space within which the optimum value must be found, by providing spatially varying surface roughness inputs in the form of land use maps (M. S. Horritt, 2000).

4.4 Comparison of Simulated Flood Extent with SAR- based Flood Maps

The predictive capability of any model needs to be assessed based on real world observations. In this study SAR based flood maps derived from the RADARSAT II image of 4th September 2003, have been used to evaluate the same. The comparison was done by comparing binary flood maps derived from the model simulations and from the SAR images. The H water depth outputs were reclassified to hold just the flooding extent information. The depth was not compared. As elaborated earlier, several approaches were used to delineate the flood boundaries. Each map was compared with the simulation results separately as well as with the aggregated possibility of inundation map.

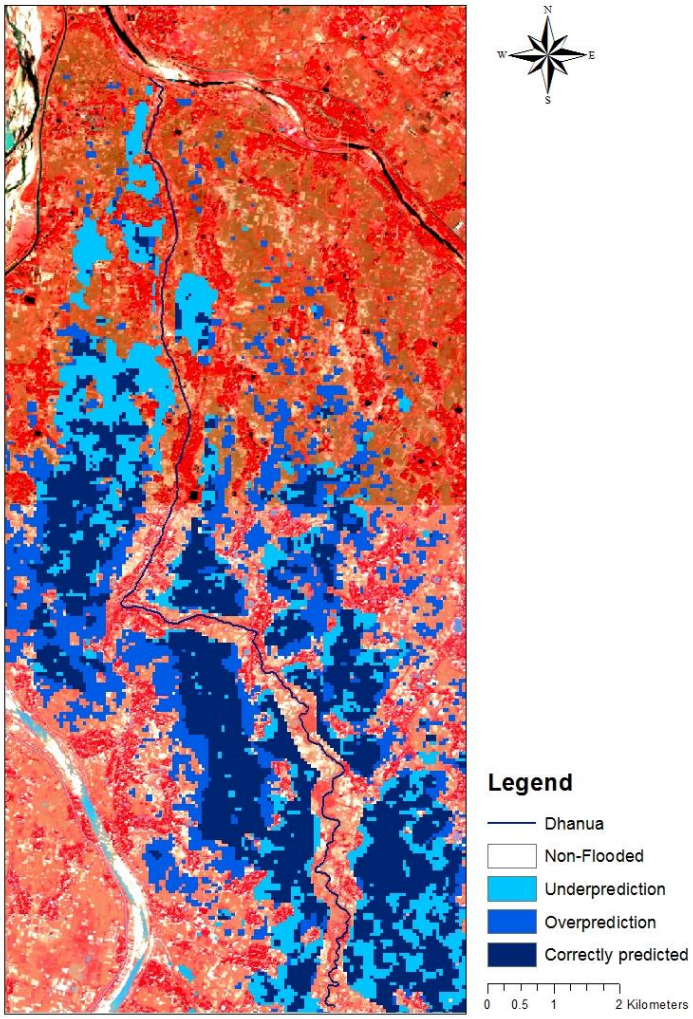

Figure 4.12: The dark blue pixels show the correctly predicted areas when compared with SAR data for the 2003 event

The SAR maps were generated from RADARSAT II and RISAT I data having spatial resolutions of 50 m and 18 m respectively. The model runs were carried out at the resolution of 15 m as higher resolution runs were much costlier in terms of simulation time and coarser resolution grids were causing loss in topographical details, eventually resulting in a loss of the predictive accuracy. Before comparison all the datasets were resampled to the resolution of the coarsest grid size in all the data used, i.e. 50 m. It has been observed in previous studies that the size, shape and configuration of the spatial aggregates can affect the results of such a comparison to a varying degree (Fischer, 2006). This issue has been termed as the Modifiable Areal Unit Problem (MAUP) due to the fact that the areal units specified in satellite imagery are not "natural" and rather arbitrary (Fischer, 2006). The MAUP may have two effects namely the zoning effect and the scale effect. The scale component acknowledges that different scales of aggregation (spatial units or pixel sizes) may reveal different patterns in the data. The effect of zonation concedes that boundaries maybe located at many different places at any given scale (Hamm, Stein, & Tolpekin, 2009). While both the effects are significant, however, for this study the scale effect is of greater consequence

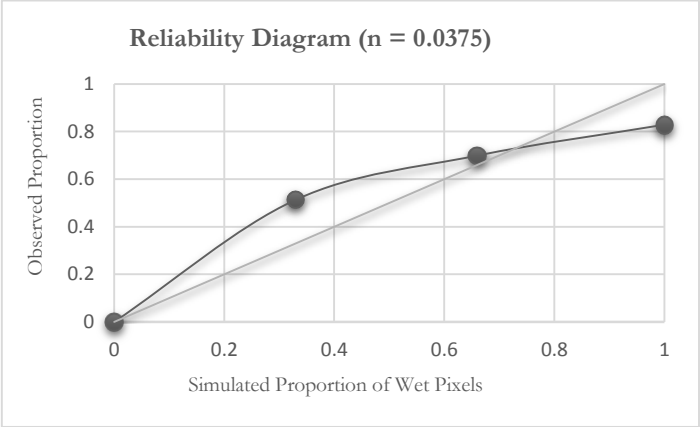

Figure 4.11: Reliability Diagram of the optimum performing bed friction parameter value.

(Paliwal, 2011). The conclusion from several studies has proven that essentially a pattern or agreement observable in the data at a particular scale may not be applicable in another. Hence, the calibration maps and the validation maps had to be at the same resolution, that of the coarsest dataset being used.

As shown in figure 4.5, the model correctly predicted most of the majorly flooded polygons but it was over-predicting (flooded in model domain but not in SAR) in some areas and under-predicting (flooded in SAR but not in the model domain) in others. On the right side of the channel, the model seems to be predicting heavy flooding, whereas the observations illustrate otherwise. The chief reason for this over prediction can be that the model is unable to drain the water from the domain due to very low slope percentages. However, in reality the water may recede earlier from that side due to other drainage channels. On the left of the channel some under prediction is observed but it can be attributed to the fact that remote sensing data (SAR) has been known to over-estimate flooding (M.S. Horritt, 2006). The reason for this is mainly that it is impossible to differentiate between the flooding being caused by the channel over-topping and the water-logging due to precipitation causing. The average gradient of elevation in the study area is so low that rain water is also impeded in such a way that water-logging is prevalent. As the model can only simulate the flood from the channel over-topping the effects of the waterlogging due to rainfall that cannot be isolated and removed from the SAR flood maps is missed by the simulated inundation extent.

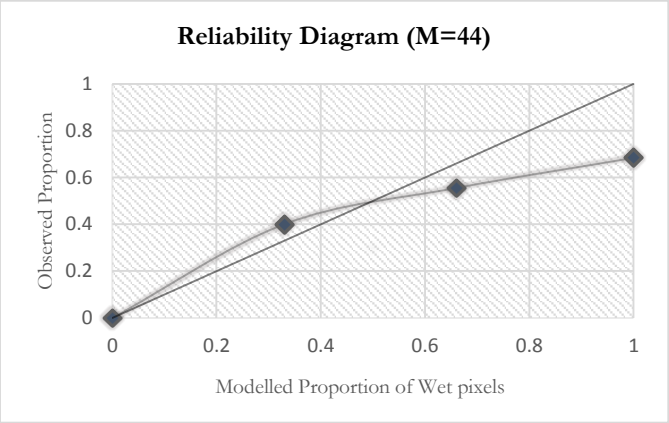

Figure 4.14: Reliability Diagram of the optimum performing floodplain friction parameter value

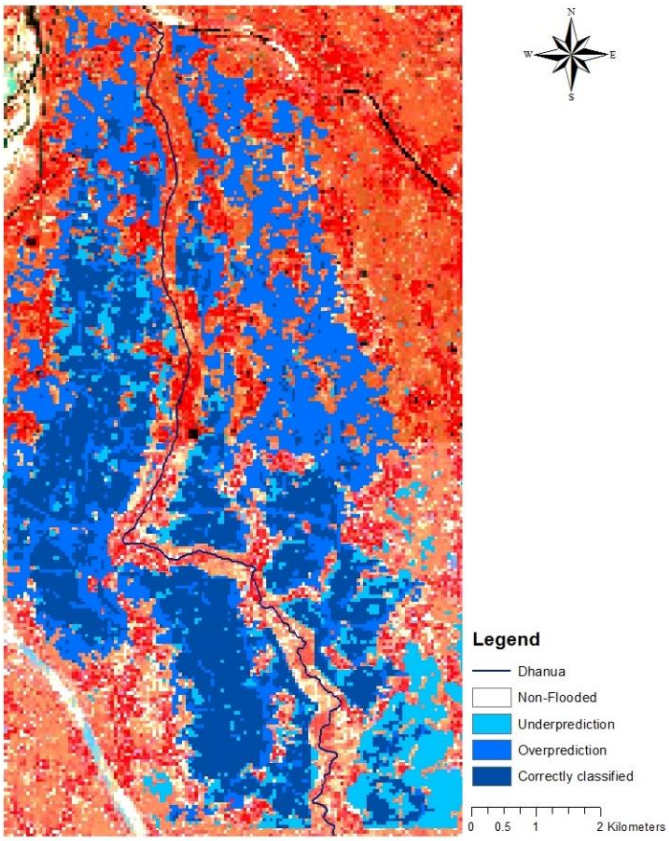

Figure 4.13: Validation map based on 9th August, 2014

Reliability diagrams were used to assess the model's performance with respect to a specific parameter as proposed by M.S. Horritt, in 2006 and elaborated in 3.4.4.2 of this thesis. The uncertain flood maps were all used to decide the best performing parameter set. A 1:1 line was used to assess the deviations from observed outputs. The minimum RMSE value of 0.254 was obtained for the value of n equal to 0.0375. Figure 4.6 illustrates the relationship between the simulated and modelled proportions of flooded pixels. The value of R^2 was found to be 0.895. As shown in figure 4.8 for the flood plain calibration the minimum RMSE value of 0.340 was observed at an M value of 44. The value of R^2 was found to be 0.912 for this relation.

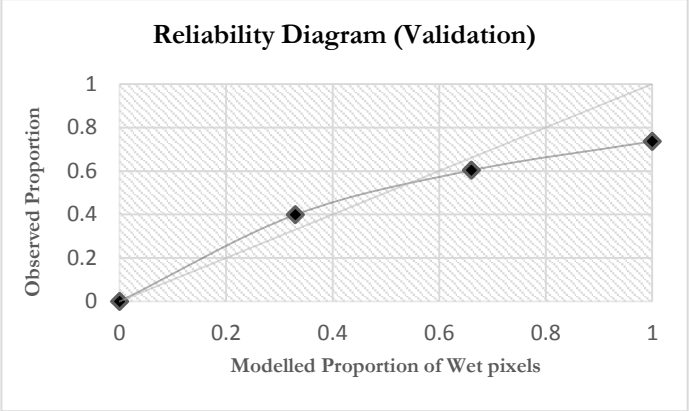

Figure 4.15: Reliability diagram of the validation run

Figure 4.15 depicts the final results of the validation run. The model is still found to be over-predicting in the right hand side of the channel but there was some under prediction in the lower right side of the channel which was not observed for the 2003 event. The reason for this can be attributed to the reason that the model was calibrated on a very big flood event with much higher discharge as compared to the discharge in the validation event. This may be the cause for the discrepancy. Figure 4.14 illustrates the reliability diagram showing the relationship between the possibility of inundation and the ideal 1:1 line. The value of R^2 was found to be equal to 0.938 and the RMSE was found to be 0.278. The model is successfully able to capture the flooding pattern in the study area which is a major improvement over previous studies (Jaipurkar, 2014) and the primary target.

Table 4.3: Summary of final results for Calibration and Validation

Calibration Parameter	R^2	RMSE
Manning's n (bed friction)	0.895	0.254
Manning's M (floodplain friction)	0.912	0.340
Validation	0.938	0.278

4.5 Reduction of Uncertainties

In order to assess and reduce the uncertainty in the model and the input data, it must first be recognised. The reason why a complex mapping approach was chosen in this study, as opposed to a simple radiometric thresholding of the SAR images, is because the subjectivity in choosing a flood delineation technique has to be acknowledged in order to remove it. By taking into consideration, all the flood maps that can be derived from SAR using various techniques, we have effectively eliminated the apparent bias that would have been introduced by choosing one method over the other without sufficient scientific backing.

As proposed in the section 3.4.5, a small ensemble of 35 simulations were used in this study to calibrate the model and assess the uncertainties. The altimetric uncertainty of the DEM was constrained to ± 2.53 m using GCPs. The uncertainty was reduced by 85.12% in comparison to the 15 m DEM generated using only the RPCs. The horizontal accuracy of the topography was increased to 0.175 pixels i.e. ±0.435 m. The parametric uncertainty in the bed friction Manning's n values was reduced from the range of ±0.01 (0.03-0.04) to 0.03725 ±0.00171, constrained by 82.9%. The flood plain friction Manning's M values were constrained to 44 ± 2.

Table 4.4: Final table of Uncertainty Reduction

Parameter	**Final value**	**Prior Uncertainty Band**	**Reduced Uncertainty Band**	**Percentage Reduction in Uncertainty**
Bed friction (Manning's n)	0.0375	±0.01	±0.00171	82.9 %.
Floodplain Friction (Manning's M)	44	±8.33	± 2	76 %
DEM (vertical)	n/a	± 17 m	± 2.53 m	85.12%
DEM (horizontal)	n/a	± 05 m	± 0.625 m	87.50%

Tarekegn (2009b), also obtained similar results for 2D modelling with an ASTER DEM in which the river terrain geometry was burned into the elevation model using an interpolation surface derived from ground surveyed channel bottom elevations. This indicated that adding ground information to satellite elevation models may indeed improve their suitability for hydrological applications. Evans, Ramachandran, Zhang, Bailey, & Cheng, (2008), also found in their study that CARTOSAT DEM accuracies are better than ASTER for most areas and comparable to SRTM. Since, they are of much higher resolution than SRTM, this finding corroborates that they can perform better for hydrodynamic modelling.

5. CONCLUSIONS AND RECOMMENDATIONS

5.1 Conclusions

The main objective of this study was to calibrate a 1D2D - coupled hydrodynamic model to simulate the flooding extent as observed from SAR data and to the reduce uncertainty in the results. The most important issue with this study was the unavailability of the ground based river cross section data and hydrometric data such as river flow and stage at various points, hence the flood inundation extent was chosen to be the calibration target. The study area had such a low elevation gradient and such a large water spread that it was very difficult to effectively constrain the model as has been observed from previous studies (Jaipurkar, 2014). Reducing the uncertainties in modelling the channel flood was considered to be the scientific challenge in this study. Satellite data was used to parameterize the roughness and provide a suitable calibration target in the absence of hydrometric gauge data at the outlet. The upstream boundary condition was calculated effectively using discharge distribution percentages and the side weir formula in HEC-RAS.

The study area conceptualization was done in such a way that it would allow for an improved understanding of the actual nature of the flooding in low lying delta regions of the Mahanadi river basin. The use of SAR data helped to overcome the hydrometric data scarcity which caused the inability to investigate in depth, the regional flooding problem. The use of high resolution optical data helped in the distributed parameterization of the floodplain roughness.

Flood extents were derived from SAR imagery using a variety of techniques based on which a possibility of inundation map was created which was based on the possibility of flooding of each pixel. Based on the ratio between the pixels that were correctly classified in each class, the model performance was assessed using reliability diagrams. The model's sensitivity to the downstream condition was tested and it was found to be very high for the regions close to location of the boundary but reduced as we moved away from it. The model becomes independent at 7.328 km upstream from the point of application of channel end boundary condition. A sensitivity analysis was also carried out for the flood plain and bed friction coefficients. The model is found to be extremely sensitive to flood plain friction but as we decrease the roughness beyond a certain point (>50 Manning's M) the model becomes independent of this parameter as well. The bed friction values showed a greater sensitivity throughout the testing range (0.01-0.1).

GIS operations were applied to optimize the DEM for modelling. Cross sections were taken at intervals of 500 m for a 19.2 km long reach. The bottom heights of the channel were used to interpolate the river bathymetry accurately so that the flow would be properly channelled. The DEM accuracy was assessed as both, a spatially varying value of vertical RMSE and a uniform vertical RMSE which was constrained to ± 2.53 m. The optimized DEM was used as the bathymetric input in the MIKE FLOOD Coupled Hydrodynamic model. The SAR based flood maps were derived using three different approaches for both the calibration and validation event, for comparison. The maps were compared using the spatial calibration statistics as elaborated in section 3.4.5. The channel and flood plain friction were calibrated using the SAR based flood maps of 2003 as reference. The results were validated against the flood maps for the 2014 flooding event.

From the aforementioned analyses it was found that uniform parameterization of the channel and floodplain friction was giving results equivalent to distributed values due to the apparent uniformity of the land use. The model was found to be consistently over-estimating in some areas due to the very low slope values. There were also specific areas always being under-predicted, this is attributed to the fact that the low elevation gradient deters the quick movement of the rain water stored and the model cannot simulate these patches.

The study shows that by constraining uncertainty in the DEM, the further propagation of errors can be curbed to a great extent. The results show a significant improvement over online free DEMs and even from the RPC CARTOSAT DEM generated from the stereo-pair. Previous studies have shown that using a high resolution DEM, water levels can be derived using the hydraulic coherence algorithm which functions on the assumption that water levels decrease from upstream to downstream. The range of DEM values underneath the flooded pixels in the channel, after the removal of uncertain pixels is considered as the true range within which the water level must lie and a feed forward algorithm is used to estimate the final values which can be used for distributed calibration to further improve the accuracy of the model (Hostache et al., 2009).

This study was the first to successfully simulate the floods in the study area as previous studies could not explain the flooding properties adequately. This proves that even data scarcity and difficult low lying terrain can be handled using detailed topographical information. Constraining the errors in the elevation information helps to reduce the uncertainty in the entire model as the terrain is the most important input of hydrodynamic modelling.

5.2 Recommendations

A major constraint in the study was the time available. Even though the channel is modelled in 1D, since the 2D results have to be written to a file at each time step, the simulation time for 1D2D models is a big constraint. This is the reason why even though higher resolution elevation data was available and studies have proven that higher the domain resolution better the results, it could not be used. The calibration was also done in a very simplistic manner due to the same reason, that there was no time to run a large ensemble of Monte Carlo Simulations. The study area houses very poor farmers who incur heavy losses annually due to the flooding problem. Thus, it is imperative that a more detailed study of this area is carried out. Keeping the above factors in mind the following recommendations are made for future research:

1. The use of the Generalized Likelihood Uncertainty Estimation technique for the parametric uncertainty estimation of the flood model. Monte Carlo simulations have proven to be an excellent technique to find the equifinal parameter sets and they should be utilized in this study area.
2. SAR derived water levels should be integrated with the model for spatially distributed calibration targets in the 1D model for the channel flow. As the model MIKE FLOOD couples the 1D and 2D models after the setup is complete, the 1D model and 2D model can be independently calibrated and then calibrated together to further improve upon the model's predictive capabilities.
3. The water levels can also be assimilated within the 1D model, to improve the model performance. Since, it is the 1D model that runs first at each time step and then it is checked if any of the cross sections are being breached and the water is transferred to the 2D model, the more accurately the 1D flow is simulated the more accurate the flooding extent in 2D will be. The breaches would occur at the correct places at correct times and the parameterization of the 2D component would become much easier.
4. Given that the region is annually flooded, the density of the hydrometric gauge networks should also be significantly increased so that along with calibrating the flooding extent, the water balance can also be effectively closed. Closing the water balance effectively is the true test of a good model and right now that cannot be verified due to the unavailability of gauges.
5. As the elevation of the area is so low and the channel is flooded every year, embankments higher than the maximum water level simulated from the probable maximum flood scenario should be built alongside the channel. This will help to effectively contain most of the water within the channel, thereby preventing future flooding events. This can be done as part of a participatory rural development program so that it requires minimum investment from the government, provides employment to the village folk as well as help in flood mitigation.

LIST OF REFERENCES

Abebe, N. a., Ogden, F. L., & Pradhan, N. R. (2010). Sensitivity and uncertainty analysis of the conceptual HBV rainfall–runoff model: Implications for parameter estimation. *Journal of Hydrology*, *389*(3-4), 301–310. doi:10.1016/j.jhydrol.2010.06.007

Al-Ali, M. S. (2011). *Assessment of high resolution SAR imagery for mapping floodplain water bodies : a comparison between Radarsat-2 and TerraSAR-X*. Durham University. Retrieved from http://etheses.dur.ac.uk/3347/

Alemsged, T. H. (2005). *Integration hydrodynamic models and high resolution DEM (LiDAR) for flood modelling*. Faculty of Earth Observation and Geo-Information Science, ITC.

Asokan, S. M., & Dutta, D. (2008). Analysis of water resources in the Mahanadi River Basin , India under projected climate conditions. *Hydrological Processes*, *22*, 3589–3603. doi:10.1002/hyp.6962

Baldassarre, G. Di, & Schumann, G. (2011). Recent advances in mapping and modelling flood processes in lowland areas. *Physics and Chemistry of the Earth, Parts A/B/C*, *36*(7-8), 221–222. doi:10.1016/j.pce.2011.03.009

Bates, P. D. (2012). Integrating remote sensing data with flood inundation models: how far have we got? *Hydrological Processes*, *26*(16), 2515–2521. doi:10.1002/hyp.9374

Bates, P. D., & De Roo, A. P. J. (2000). A simple raster-based model for flood inundation simulation. *Journal of Hydrology*, *236*(1-2), 54–77.

Bates, P. D., Horritt, M. S., Aronica, G., & Beven, K. (2004). Bayesian updating of flood inundation likelihoods conditioned on flood extent data. *Hydrological Processes*, *18*(17), 3347–3370. doi:10.1002/hyp.1499

Beven, K. (1993). Prophecy , reality and uncertainty in distributed hydrological modelling. *Advances in Water Resources*, *16*(1), 41–51.

Beven, K., & Binley, A. (1992). The Future of Distributed Models: Model Calibration and Uncertainty Prediction. *Hydrological Processes*. doi:10.1002/hyp.3360060305

Carrivick, J. L. (2006). Application of 2D hydrodynamic modelling to high-magnitude outburst floods: An example from Kverkfjöll, Iceland. *Journal of Hydrology*, *321*(1-4), 187–199. doi:10.1016/j.jhydrol.2005.07.042

Chatterjee, C., Forster, S., & Bronstert, A. (2008). Comparison of hydrodynamic models of different complexities to model floods with emergency storage areas. *Hydrological Processes*, *22*(24), 4695–4709. doi:10.1002/hyp.7079

DeChant, C. M. (2014). *Quantifying the Impacts of Initial Condition and Model Uncertainty on Hydrological Forecasts*. Portland State University. Retrieved from http://pdxscholar.library.pdx.edu/cgi/viewcontent.cgi?article=2797&context=open_access_etds

DHI. (2014a). *MIKE 11 - User's Manual* (pp. 278–325).

DHI. (2014b). *MIKE FLOOD* (pp. 1–162). Danish Hydraulic Institute.

DHI. (2014c). *MIKE11 - Reference Manual* (8th ed.). Danish Hydraulic Institute.

Di Baldassarre, G., Schumann, G., & Bates, P. D. (2009). A technique for the calibration of hydraulic models using uncertain satellite observations of flood extent. *Journal of Hydrology*, *367*(3-4), 276–282. doi:10.1016/j.jhydrol.2009.01.020

Dimet, L., Castaings, W., Ngnepieba, P., & Vieux, B. (2009). *Data Assimilation for Atmospheric, Oceanic and Hydrologic Applications*. (S. K. Park & L. Xu, Eds.) (pp. 367–405). Berlin, Heidelberg: Springer Berlin Heidelberg. doi:10.1007/978-3-540-71056-1

Euskal, U., Agencia, A., & Ura, A. (n.d.). Keywords: real time flood forecast system, Distributed hydrology MIKE SHE-MIKE11.

Evans, G. a, Ramachandran, B., Zhang, Z., Bailey, G. B., & Cheng, P. (2008). An Accuracy Assessment of Cartosat-1 Stereo Image Data-Derived Digital Elevation Models : A Case Study of the Drum Mountains , Utah. *XX1st ISPRS Congress*, 1161–1164. Retrieved from www.isprs.org/proceedings/XXXVII/congress/1_pdf/198.pdf?

Fischer, M. M. (2006). Spatial Analysis in Geography. In *Spatial Analysis and Geocomputation* (pp. 17–28). Springer Berlin Heidelberg. doi:10.1007/3-540-35730-0_2

Gilles, D., & Moore, M. (2010). Review of Hydraulic Flood Modeling Software used in Belgium , The Netherlands , and The United Kingdom. *International Perspectives in Water Resource Management*.

Giustarini, L., Matgen, P., Hostache, R., Montanari, M., Plaza, D., Pauwels, V. R. N., … Savenije, H. H. G. (2011). Assimilating SAR-derived water level data into a hydraulic model: a case study. *Hydrology and Earth System Sciences*, *15*(7), 2349–2365. doi:10.5194/hess-15-2349-2011

Gumindoga, W., Rwasoka, D. T., & Murwira, a. (2011). Simulation of streamflow using TOPMODEL in the Upper Save River catchment of Zimbabwe. *Physics and Chemistry of the Earth, Parts A/B/C*, *36*(14-15), 806–813. doi:10.1016/j.pce.2011.07.054

Haile, A. T. (2005). *Integrating Hydrodynamic Models and High Resolution DEM(LIDAR) For Flood Modelling*. University of Twente. Retrieved from www.itc.nl/library/papers_2005/msc/wrem/haile.pdf

Haile, A. T., & Rientjes, T. H. M. (2005). EFFECTS OF LIDAR DEM RESOLUTION IN FLOOD MODELLING : A MODEL SENTITIVITY STUDY FOR THE CITY OF TEGUCIGALPA , HONDURAS. In *ISPRS WG III/3, III/4, V/3 Workshop "Laser scanning 2005", Enschede, The Netherlands* (pp. 168–173).

Haile, A. T., & Rientjes, T. H. M. (2007). Uncertainty Issues in Hydrodynamic Flood Modeling. In *Proceedings of the 5th International symposium on Spatial Data Quality SDQ 2007, Modelling qualities in space and time, ITC, Enschede, The Netherlands, 13–15 June 2007*.

Hamm, N. A. S., Stein, A., & Tolpekin, V. (2009). Analyzing the Effect of the Modifiable Areal Unit Problem in Remote Sensing: Short Note. In R. Devillers & H. Goodchild (Eds.), *Spatial data quality : from process to decisions* (p. 179). CRC / Taylor & Francis.

Horritt, M. S. (2000). Calibration of a two-dimensional finite element flood flow model using satellite radar imagery. *Water Resources Research*, *36*(11), 3279–3291.

Horritt, M. S. (2006). A methodology for the validation of uncertain flood inundation models. *Journal of Hydrology*, *326*(1-4), 153–165. doi:10.1016/j.jhydrol.2005.10.027

Horritt, M. S., & Bates, P. D. (2002). Evaluation of 1D and 2D numerical models for predicting river flood inundation. *Journal of Hydrology*, *268*, 87–99.

Hostache, R., Lai, X., Monnier, J., & Puech, C. (2010). Assimilation of spatially distributed water levels into a shallow-water flood model. Part II: Use of a remote sensing image of Mosel River. *Journal of Hydrology*, *390*(3-4), 257–268. doi:10.1016/j.jhydrol.2010.07.003

Hostache, R., Matgen, P., Schumann, G., Puech, C., Hoffmann, L., & Pfister, L. (2009). Water Level Estimation and Reduction of Hydraulic Model Calibration Uncertainties Using Satellite SAR Images of Floods. *IEEE Transactions on Geoscience and Remote Sensing*, (February), 1–10.

Hostache, R., Schumann, G., Matgen, P., Puech, C., Hoffmann, L., & Pfister, L. (2006). 3D Flood Information from SAR as a mean for Reducing Uncertainties in Flood Inundation Modelling. In *XXX ISPRS Congress, Commission VII* (pp. 217–222).

Hunter, N. M., Bates, P. D., Horritt, M. S., & Wilson, M. D. (2007). Simple spatially-distributed models for predicting flood inundation: A review. *Geomorphology*, *90*(3-4), 208–225. doi:10.1016/j.geomorph.2006.10.021

Jaipurkar, P. K. (2014). *2D Hydrodynamic modelling on part of Mahanadi Delta Region*.

Jayachandraiah, B., Krishnan, S. M., Srinivas, V., & Kumar, A. S. (2007). SPATIAL AND RADIOMETRIC CHARACTERISTICS OF CARTOSAT-1. In *Commission IV, WG IV/9* (pp. 5–8).

Jung, H. C., Jasinski, M., Kim, J.-W., Shum, C. K., Bates, P., Neal, J., … Alsdorf, D. (2012). Calibration of two-dimensional floodplain modeling in the central Atchafalaya Basin Floodway System using SAR interferometry. *Water Resources Research*, *48*(7), n/a–n/a. doi:10.1029/2012WR011951

Koriche, S. A. (2012). *Remote Sensing Based Hydrological Modelling for Flood Early Warning in the Upper and Middle Awash River Basin*. University of Twente. Retrieved from www.itc.nl/library/papers_2012/msc/wrem/koriche.pdf

Li, J., & Wong, D. W. S. (2010). Effects of DEM sources on hydrologic applications. *Computers, Environment and Urban Systems*, *34*(3), 251–261. doi:10.1016/j.compenvurbsys.2009.11.002

Mani, P., Chatterjee, C., & Kumar, R. (2013). Flood hazard assessment with multiparameter approach derived from coupled 1D and 2D hydrodynamic flow model. *Natural Hazards*, *70*(2), 1553–1574. doi:10.1007/s11069-013-0891-8

Mason, D. C., Bates, P. D., & Dall' Amico, J. T. (2009). Calibration of uncertain flood inundation models using remotely sensed water levels. *Journal of Hydrology*, *368*(1-4), 224–236. doi:10.1016/j.jhydrol.2009.02.034

Matgen, P., Henry, J.-B., Pappenberger, F., de Fraipont, P., Hoffmann, L., & Pfister, L. (2004). Uncertainty in Calibrating Flood Propagation Models with Flood Boundaries Derived from SAR Imagery. In *XX ISPRS Congress, Commission VII*.

Matgen, P., Montanari, M., Hostache, R., Pfister, L., Hoffmann, L., Plaza, D., … Savenije, H. H. G. (2010). Towards the sequential assimilation of SAR-derived water stages into hydraulic models using the Particle Filter: proof of concept. *Hydrology and Earth System Sciences*, *14*(9), 1773–1785. doi:10.5194/hess-14-1773-2010

Matgen, P., Schumann, G., Henry, J.-B., Hoffmann, L., & Pfister, L. (2007). Integration of SAR-derived river inundation areas, high-precision topographic data and a river flow model toward near real-time flood management. *International Journal of Applied Earth Observation and Geoinformation*, *9*(3), 247–263. doi:10.1016/j.jag.2006.03.003

Merwade, V., Cook, A., & Coonrod, J. (2008). GIS techniques for creating river terrain models for hydrodynamic modeling and flood inundation mapping. *Environmental Modelling & Software*, *23*(10-11), 1300–1311. doi:10.1016/j.envsoft.2008.03.005

Montanari, M., Hostache, R., Matgen, P., Schumann, G., Pfister, L., & Hoffmann, L. (2009). Calibration and sequential updating of a coupled hydrologic-hydraulic model using remote sensing-derived water stages. *Hydrology and Earth System Sciences*, *13*(3), 367–380. doi:10.5194/hess-13-367-2009

Moore, M. R. (2011). *Development of a high-resolution 1D/2D coupled flood simulation of Charles City, Iowa*. University of Iowa. Retrieved from http://ir.uiowa.edu/etd/1032/

Moradkhani, H., Hsu, K.-L., Gupta, H., & Sorooshian, S. (2005). Uncertainty assessment of hydrologic model states and parameters: Sequential data assimilation using the particle filter. *Water Resources Research*, *41*(5), n/a–n/a. doi:10.1029/2004WR003604

Murthy, Y. V. N. K., Rao, S. S., Rao, D. S. P., & Jayaraman, V. (2008). Analysis of DEM generated using Cartosat-1 stereo data over Mausanne Les Alpiles - Cartosat Scientific Appraisal Programme (CSAP TS-5). *The International Archives of the Photogrammetry, Remote Sensing and Spatial Information Sciences*, *XXXVII*(Figure 1), 1–6.

Noh, S. J. I. N., Tachikawa, Y., Shiiba, M., & Kim, S. (2013). Sequential data assimilation for streamflow forecasting using a distributed hydrologic model : particle filtering and ensemble Kalman filtering. *Floods: From Risk to Opportunity*, *357*, 341–349.

Paliwal, A. (2011). *The impact of modifiable areal unit problem on estimation of lake extent*. University of Twente. Retrieved from www.itc.nl/library/papers_2011/msc/gem/paliwal.pdf

Patro, S., Chatterjee, C., Mohanty, S., Singh, R., & Raghuwanshi, N. S. (2009). Flood Inundation Modeling using MIKE FLOOD and Remote Sensing Data. *Journal Indian Society of Remote Sensing*, *37*(March), 107–118.

Patro, S., Chatterjee, C., Singh, R., & Raghuwanshi, N. S. (2009). Hydrodynamic modelling of a large flood-prone river system in India with limited data. *Hydrological Processes*, *23*(July), 2774–2791. doi:10.1002/hyp.7375

Priestnall, G., Jaafar, J., & Duncan, a. (2000). Extracting urban features from LiDAR digital surface models. *Computers, Environment and Urban Systems*, *24*(2), 65–78. doi:10.1016/S0198-9715(99)00047-2

Puech, C., Hostache, R., Raclot, D., & Matgen, P. (2007). Estimation of flood water levels by merging DEM and satellite imagery using hydraulics laws through AI to enhance the estimates. In *Proceedings of Second Space for Hydrology Workshop. ESA.* (pp. 1–7). Geneva.

Rientjes, T. H. M., Haile, a. T., Kebede, E., Mannaerts, C. M. M., Habib, E., & Steenhuis, T. S. (2011). Changes in land cover, rainfall and stream flow in Upper Gilgel Abbay catchment, Blue Nile basin – Ethiopia. *Hydrology and Earth System Sciences*, *15*(6), 1979–1989. doi:10.5194/hess-15-1979-2011

Sanders, B. F. (2007). Evaluation of on-line DEMs for flood inundation modeling. *Advances in Water Resources*, *30*(8), 1831–1843. doi:10.1016/j.advwatres.2007.02.005

Sanyal, J., & Lu, X. X. (2004). Application of Remote Sensing in Flood Management with Special Reference to Monsoon Asia: A Review. *Natural Hazards*, *33*(2), 283–301. doi:10.1023/B:NHAZ.0000037035.65105.95

Sanyal, J., & Lu, X. X. (2005). Remote sensing and GIS-based flood vulnerability assessment of human settlements: a case study of Gangetic West Bengal, India. *Hydrological Processes*, *19*(18), 3699–3716. doi:10.1002/hyp.5852

Schumann, G., Bates, P. D., Horritt, M. S., Matgen, P., & Pappenberger, F. (2009). Progress in integration of remote sensing-derived flood extent and stage data and hydraulic models. *Reviews of Geophysics*, *47*(2008), 1–20. doi:10.1029/2008RG000274

Schumann, G., Di Baldassarre, G., & Bates, P. D. (2009). The utility of spaceborne radar to render flood inundation maps based on multialgorithm ensembles. *IEEE Transactions on Geoscience and Remote Sensing*, *47*(8), 2801–2807. doi:10.1109/TGRS.2009.2017937

Schumann, G., Matgen, P., Hoffmann, L., Hostache, R., Pappenberger, F., & Pfister, L. (2007). Deriving distributed roughness values from satellite radar data for flood inundation modelling. *Journal of Hydrology*, *344*(1-2), 96–111. doi:10.1016/j.jhydrol.2007.06.024

Schumann, G., Pappenberger, F., & Matgen, P. (2008). Estimating uncertainty associated with water stages from a single SAR image. *Advances in Water Resources*, *31*(8), 1038–1047. doi:10.1016/j.advwatres.2008.04.008

Singh, S. K. (2004). *Analysis of Uncertainties In Digital Elevation Models in Flood (Hydraulic) Modelling*.

Singh, V. K., Ray, P. K. C., & Jeyaseelan, A. P. T. (2010). Orthorectification and Digital Elevation Model (DEM) Generation Using Cartosat-1 Satellite Stereo Pair in Himalayan Terrain. *Journal of Geographic Information System*, *02*(02), 85–92. doi:10.4236/jgis.2010.22013

Slivinski, L., Spiller, E., & Apte, A. (2015). A Hybrid Particle-Ensemble Kalman Filter for Lagrangian Data Assimilation. *Monthly Weather Review*, *143*(1), 195–211. doi:http://dx.doi.org/10.1175/MWR-D-14-00051.1

Srivastava, P. K., Srinivasan, T. P., Gupta, A., Singh, S., Nain, J. S., Prakash, S., … Krishna, B. G. (2007). RECENT ADVANCES IN CARTOSAT-1 DATA PROCESSING. *ISPRS Hannover Workshop*, (May 2005).

Stephens, E. M., Bates, P. D., Freer, J. E., & Mason, D. C. (2012). The impact of uncertainty in satellite data on the assessment of flood inundation models. *Journal of Hydrology*, *414-415*, 162–173. doi:10.1016/j.jhydrol.2011.10.040

Tarekegn, T. H. (2009a). *Modelling Using ASTER DEM ; the case of Ribb*.

Tarekegn, T. H. (2009b). *Two Dimensional Hydrodynamic Flood Modelling Using ASTER DEM ; the case of Ribb Catchment, Ethiopia*.

Tarekegn, T. H., Haile, A. T., Rientjes, T., Reggiani, P., & Alkema, D. (2010). Assessment of an ASTER-generated DEM for 2D hydrodynamic flood modeling. *International Journal of Applied Earth Observation and Geoinformation*, *12*(6), 457–465. doi:10.1016/j.jag.2010.05.007

Vanderkimpen, P., Melger, E., & Peeters, P. (2009). Flood modeling for risk evaluation – a MIKE FLOOD vs . SOBEK 1D2D benchmark study. *Flood Risk Management: Research and Practice*, 77–84.

Werner, M. G. F., Hunter, N. M., & Bates, P. D. (2005). Identifiability of distributed floodplain roughness values in flood extent estimation. *Journal of Hydrology*, *314*(1-4), 139–157. doi:10.1016/j.jhydrol.2005.03.012

Wu, S., Li, J., & Huang, G. H. (2008). A study on DEM-derived primary topographic attributes for hydrologic applications: Sensitivity to elevation data resolution. *Applied Geography*, *28*(3), 210–223. doi:10.1016/j.apgeog.2008.02.006

Yamazaki, D., Baugh, C. a., Bates, P. D., Kanae, S., Alsdorf, D. E., & Oki, T. (2012). Adjustment of a spaceborne DEM for use in floodplain hydrodynamic modeling. *Journal of Hydrology*, *436-437*, 81–91. doi:10.1016/j.jhydrol.2012.02.045

APPENDIX I: CROSS SECTION DATA

The cross sections collected on field were done using a rapid GPS surveying of the levee and river bank points, while the channel depth was estimated using a measuring pole. The cross sections were extracted from the 5 m bathymetry file using the GIS interface in the MIKE FLOOD model called MIKE HYDRO. Since the reach was about 19.2 km and there were only 6 surveyed cross-sections we had to rely more on the DEM. As the terrain properties were changing very little with distance, a more extensive ground cross section survey was not considered necessary for the purpose of this study, considering the total time available for research. The cross sections were drawn in MIKE HYDRO and their elevations extracted from the DEM and care was taken to draw cross sections at the surveyed chainages. These were then edited in accordance with the surveyed elevations and further used to interpolate cross sections at every 200 m. The cross sections thus derived were further corrected as auto-generated cross sections sometimes have errors such as crossing each other or crossing the channel twice, etc. which causes problems in the hydraulic conveyance of the 1D model.

The table of the surveyed cross sections, supported by DEM derived elevations has been added here for future reference.

Chainage 0		Chainage 3000		Chainage 8100		Chainage 14000		Chainage 10800		Chainage 15900	
X	Z	X	Z	X	Z	X	Z	X	Z	X	Z
0	19.6	2	18.0	46	17.2	0	13.8	36	14.9	37	13.1
2	19.6	47	18.4	57	17.2	13	13.8	38	14.9	54	13.1
36	19.8	47	18.4	57	17.2	21	13.8	44	15.0	61	13.1
40	19.9	71	18.6	70	17.0	21	13.8	53	15.1	69	13.1
42	20.1	83	18.8	84	16.7	32	13.7	60	15.2	81	13.0
43	20.2	87	18.9	97	16.4	51	13.8	60	15.2	88	12.8
45	20.4	99	20.0	124	15.6	51	13.8	67	15.4	89	12.5
48	20.8	102	20.1	137	15.3	56	14.1	72	15.4	90	12.4
50	21.3	110	20.3	138	15.1	60	14.1	81	15.4	91	12.3
51	21.4	110	20.3	146	14.9	64	14.1	88	15.4	93	12.2
56	21.5	112	20.3	154	14.7	64	14.1	95	15.2	101	11.9
61	21.6	120	20.1	167	14.7	68	14.0	105	15.1	107	11.7
66	21.4	123	19.8	183	14.6	71	13.6	110	14.8	109	11.6
71	20.4	126	19.6	191	14.6	69	13.6	115	14.5	109	11.6
76	20.2	132	19.0	209	14.4	72	13.2	116	14.3	114	11.5
82	20.0	134	18.7	220	14.3	83	12.9	119	13.8	121	11.3
85	20.0	137	18.5	226	14.2	105	12.2	125	13.4	124	11.3
89	19.6	140	18.4	236	14.1	113	12.2	140	13.4	133	11.2
90	19.5	145	18.2	239	14.1	125	12.2	153	13.4	148	11.3
91	19.5	150	17.9	239	14.1	125	12.2	160	13.4	162	11.3
93	19.4	158	17.7	241	14.1	144	12.3	168	13.4	174	11.4
98	19.4	178	17.6	255	14.6	149	12.4	176	13.4	185	11.6
118	19.2	215	17.8	256	14.7	160	12.7	191	13.4	187	11.6
120	19.2	226	17.9	260	14.8	161	12.9	213	13.7	191	11.7
125	18.6	234	18.1	267	15.2	164	13.0	221	13.9	193	11.8
162	18.5	237	18.2	272	15.5	165	13.6	225	14.1	195	11.9
167	19.0	241	18.9	284	16.0	168	13.7	226	14.2	204	12.1
170	19.0	245	19.2	284	16.0	175	13.8	227	14.4	212	12.1
173	19.1	250	19.4	289	16.2	179	13.8	230	14.6	219	12.3
175	19.1	257	19.4	289	16.2	182	13.7	236	14.8	226	12.4
178	19.2	264	19.4	292	16.4	186	13.5	239	14.9	234	12.6
180	19.3	264	19.4	298	16.6	186	13.5	241	14.9	238	12.6
228	19.9	271	19.4	306	16.9	193	13.3	241	14.9	244	12.8
231	19.9	272	19.5	314	17.0	203	13.3	254	14.8	248	13.0
249	20.2	272	19.6	321	16.9	203	13.3	262	14.6		
251	20.3	273	19.8	339	16.5	213	13.3	268	14.2		
257	21.3	273	20.3	348	16.4	213	13.3	274	14.0		
259	21.5	274	20.4	358	16.2	215	13.3	278	13.7		
260	21.6	282	20.4	366	16.0	222	13.4	282	13.5		
261	21.8	291	20.3	397	15.5	230	13.4				
265	21.9	296	20.2	397	15.5	235	13.5				
271	22.2	298	20.0	408	15.5	238	13.6				
274	22.3	300	19.9								

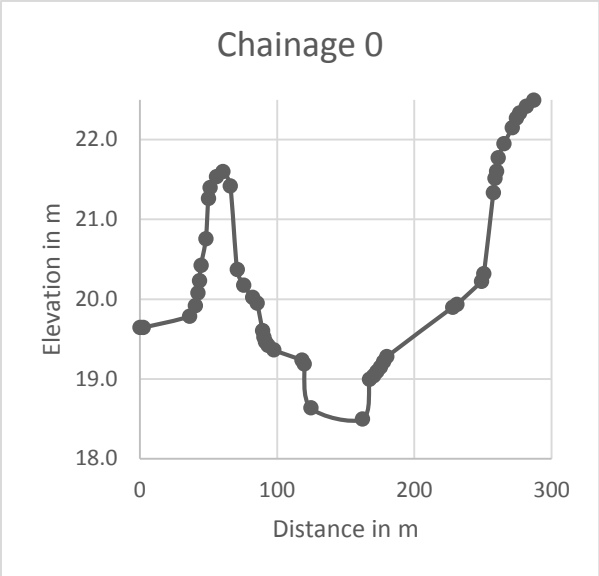
Chainage 0
Elevation in m
22.0
21.0
20.0
19.0
18.0
0
100
200
300
Distance in m

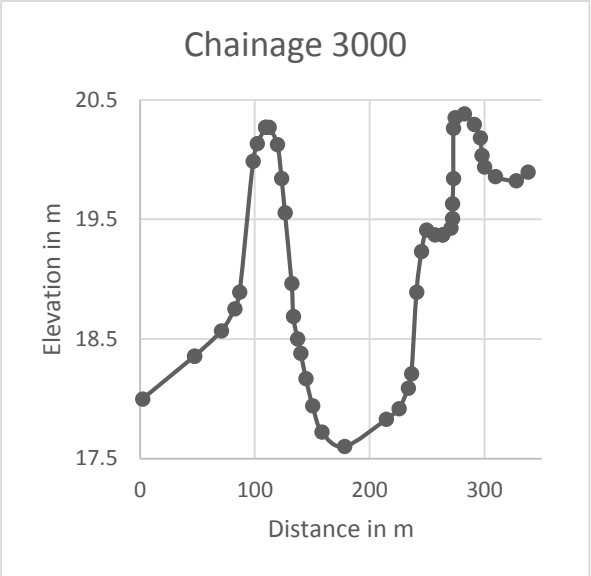
Chainage 3000
Elevation in m
20.5
19.5
18.5
17.5
0
100
200
300
Distance in m

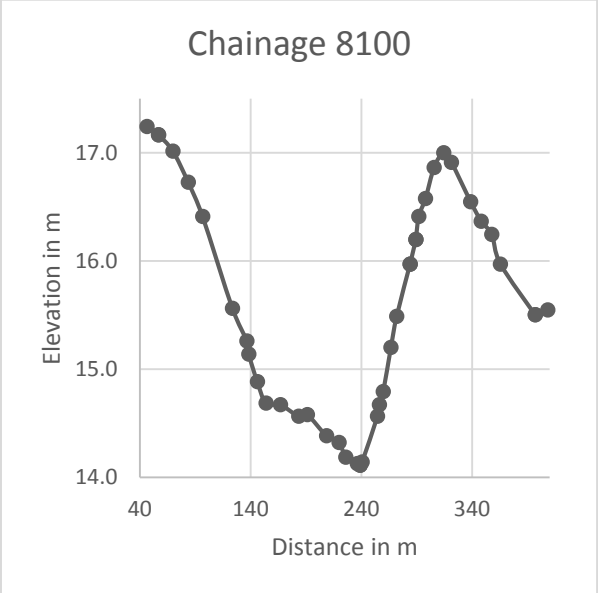
Chainage 8100
Elevation in m
17.0
16.0
15.0
14.0
40
140
240
340
Distance in m

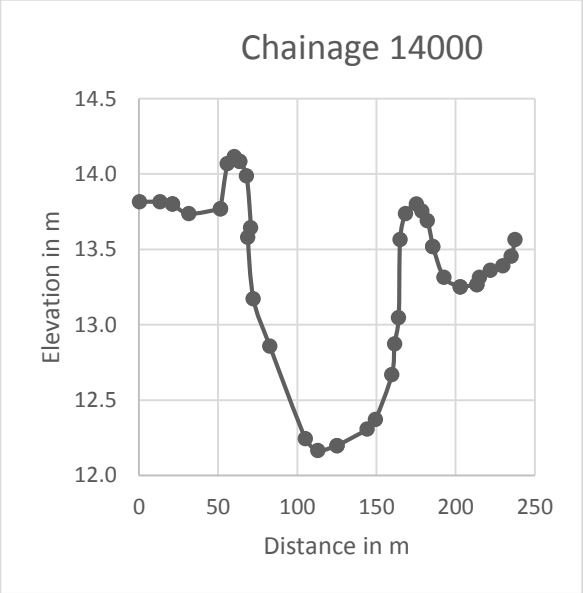
Chainage 14000
Elevation in m
14.5
14.0
13.5
13.0
12.5
12.0
0
50
100
150
200
250
Distance in m

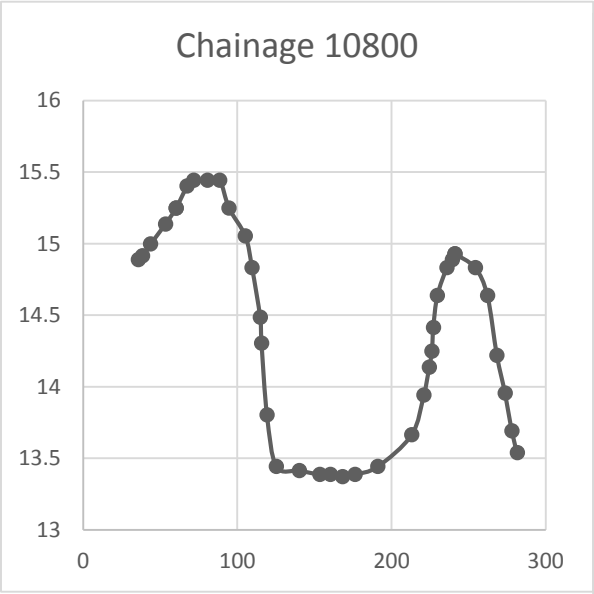
Chainage 10800
16
15.5
15
14.5
14
13.5
13
0
100
200
300

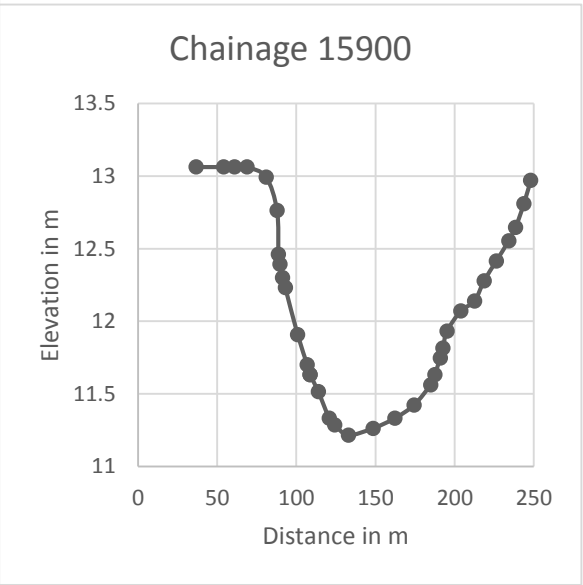
Chainage 15900
Elevation in m
13.5
13
12.5
12
11.5
11
0
50
100
150
200
250
Distance in m